Locomotion on a lubricating fluid with spatial viscosity variations

Takahiro Kanazawa[1,2,3,*] and Kenta Ishimoto[4,†]

[1]*Department of Physics, The University of Tokyo, Tokyo 113-0033, Japan*

[2]*Nonequilibrium Physics of Living Matter Laboratory, RIKEN Pioneering Research Institute, Wako 351-0198, Japan*

[3]*Department of Physics, The University of Chicago, Chicago, Illinois 60637, USA*

[4]*Department of Mathematics, Kyoto University, Kyoto 606-8502, Japan*

(Received 11 March 2025; accepted 21 July 2025; published 21 October 2025)

We study locomotion of a model crawler corresponding to a deforming upper boundary of finite length above a thin Newtonian fluid film whose viscosity varies spatially. We first derive a general locomotion velocity formula with fluid viscosity variations via the lubrication theory. For further analysis, the surface of the crawler is described by a combination of transverse and longitudinal traveling waves and we find that under a uniform viscosity a transverse wave results in a retrograde crawler, while a longitudinal wave leads to a direct crawler. We then analyze the time-averaged locomotion behaviors under two scenarios: (i) a sharp viscosity interface and (ii) a linear viscosity gradient. Using the asymptotic expansions of small surface deformations and the method of multiple timescale analysis, we derive an explicit form of the average velocity that captures nonlinear, accumulative interactions between the crawler and the spatially varying environment. (i) In the case of a viscosity interface, the time-averaged speed of the crawler is always slower than that in the uniform viscosity, for both the transverse and longitudinal wave cases. Notably, the speed reduction is most significant when the crawler's front enters a more viscous layer and the crawler's rear exits from the same layer. (ii) In the case of a viscosity gradient, the crawler's speed becomes slower for the transverse wave, while for the longitudinal wave, the locomotion speed does not change significantly. Our analysis illustrates the fundamental importance of interactions between a locomotor and its environment, and separating the timescale behind the locomotion.

DOI: 10.1103/yrzq-k45v

I. INTRODUCTION

Locomotion is a fundamental feature that animals use to survive in their environment; they walk on land, swim in water, fly in the air, and dive into porous media to search for food and mates and escape from lethal situations and predators. Here, the mechanical interaction between a deforming body and its surrounding environment is essential for the dynamics of locomotion itself [1].

Crawling, a type of locomotion by means of body deformation on a substrate, is widely seen in gastropods, arthropods, snakes, caterpillars, and earthworms [2–6]. The mechanical interactions

*Contact author: kt@g.ecc.u-tokyo.ac.jp

†Contact author: kenta.ishimoto@math.kyoto-u.ac.jp

between the crawler and a substrate have been treated from different mechanical aspects as frictional forces at the substrate [7–9], viscous and viscoplastic forces [10–12], and anchoring forces [13,14]. Among these crawlers, mollusca, including gastropods, slugs, and snails, typically crawl on a substrate by deforming their elastic body covered with secreted mucus. Hence, the hydrodynamic interactions at the substrate have been a focus for these types of crawlers, and a prototypical mathematical model of such a locomotion system has been formulated as a deforming boundary on a lubricating fluid film [15,16]. These crawler dynamics have also been examined experimentally through mechanical robots [15,17,18]. In the present study, we consider locomotion of a model crawler corresponding to a deforming upper boundary of finite length above a thin Newtonian fluid film.

The deformation of these animals is typically driven by a peristaltic traveling muscular wave, and two major crawling modes are known: crawling with retrograde waves and with direct (prograde) waves [19]. A retrograde crawler, which is usually seen in marine gastropods, moves in a direction opposite to that of the traveling pedal wave, and a direct crawler is usually seen in terrestrial gastropods and moves in the same direction as the traveling wave. The type of crawling depends on the species, but interestingly, both modes can be seen in an individual when backward locomotion is induced [14,20,21]. For example, *Ischnochiton comptus* exhibits retrograde crawling for forward locomotion, and direct crawling is used for backward locomotion [14]. In both forward and backward locomotion, the deformation wave travels from head to tail.

Lubrication approximation in fluid mechanics holds when the length scales in two directions are sufficiently separated. Let us consider the typical length scales in, for example, gastropods. The typical wavelength of the pedal of snails is 10^{-3} m [22]. In contrast, the mucus thickness of gastropods is typically on the order of 10^{-5} to 10^{-4} m [11,22–24]. These can be taken as typical longitudinal (parallel to the locomotion direction) and transverse (perpendicular to the locomotion direction) length scales, respectively, to validate the use of lubrication approximation. In Chan *et al.* [15], only transverse surface deformation was considered, which resulted in a retrograde crawler with Newtonian fluids. Katz [25] addressed a similar problem and concluded that longitudinal deformation has subleading-order contribution to physical quantities in the expansion with respect to the small length ratio in a usual lubrication setting.

The models have been extended to include non-Newtonian properties of the lubricating fluids [26,27], elasticity of the body of the crawler as an elastic sheet [28–30], and both of these [31] to account for the two typical modes of crawling (i.e., with retrograde and direct waves). Other studies have explored the hydrodynamics of locomotion under a free surface [32,33] and particle collection on a water surface [34,35].

In the fluid dynamics of animal locomotion, spatial viscosity variations play an important role, such as a viscous layer on the epithelium to provide protection from infectious bacteria [36]. The spatial fluid viscosity variation is also realized by temperature variations and inhomogeneous density distribution of a solute (e.g., salt or nutrient) and solvent composition [37]. Viscotaxis [38,39], the tendency of active agents to accumulate in regions with higher or lower viscosity due to an interaction between fluids and the (active) particle, is an illustrative example of how viscosity variation provides navigation during locomotion. In the low-Reynolds number hydrodynamics of swimming, recently the effects of spatial viscosity variation or viscosity gradients on swimming behaviors have been intensively studied.

One type of spatial variation is a (small) viscosity gradient. Studies of the effects of a viscosity gradient on spherical squirmers [40–44] and spheroidal swimmers [45,46] revealed additional torques that change the swimming direction, yielding swimmer guidance. A Taylor sheet [47] in a viscosity stratified fluid was addressed in Dandekar and Ardekani [48], and they found a reduction in the swimming velocity. Moreover, resistive force theory and the scallop theorem under viscosity gradients were studied in Kamal and Lauga [49] and Esparza López and Lauga [50], respectively. Liu *et al.* [51] and Anand *et al.* [52] studied an elastic rod in a viscosity gradient in the context of ciliary motion and flagellar beating, respectively.

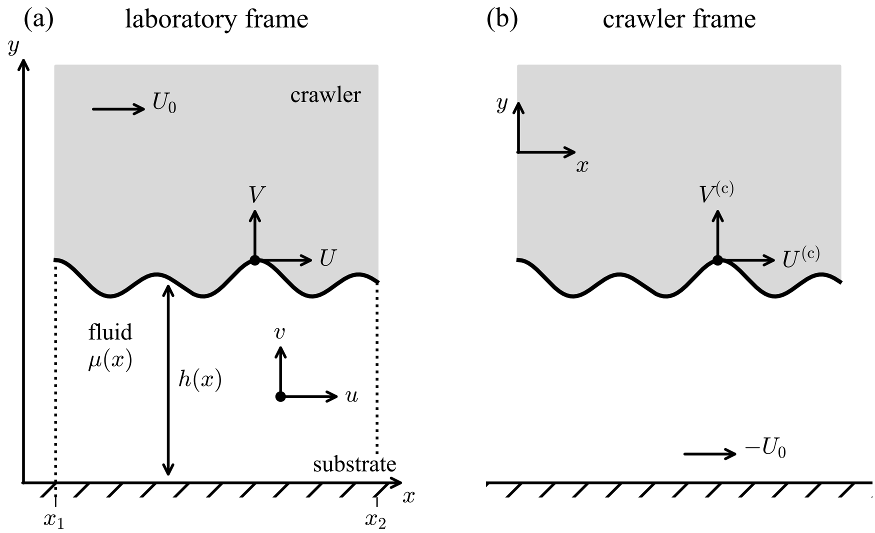

FIG. 1. Schematic of the problem setup and two reference frames: (a) the laboratory frame and (b) the frame comoving to an upper surface (crawler frame).

Another type of spatial viscosity variation can be found in a sharp interface between two fluids with different viscosities. The dynamics of helical swimmers crossing a viscosity interface were studied in Gonzalez-Gutierrez *et al.* [53] and Esparza López *et al.* [54]. Active particles crossing a sharp viscosity gradient were studied experimentally [37], computationally [55], and theoretically [56].

Because the locomotive motion is usually achieved by repeating cycles of gaits, two timescales naturally arise: the fast motion of the periodic gait and slow displacement of the entire body. When the locomotion relies on viscous resistance, as for swimming microorganisms in low-Reynolds number fluids, in particular, these two timescales are well separated due to inefficient locomotion in this environment, as seen in sperm progressive dynamics accompanied by a lateral yawing motion [57] and the back-and-forth motion of *Chlamydomonas* [58]. Such a fast oscillation coupled with the surrounding environment often yields nonlinear effects in long-term locomotion behavior, leading to the eventual turning seen in chemotaxis and phototaxis [59–62]. To deal with these multiple timescale phenomena in locomotion, the utility of multiscale analysis has recently been explored in the context of microswimmers in a complex environment, including swimmer-shear coupling [63–66], the rheotactic response of microalgae in a Poiseuille flow [67], and swimmer-wall and swimmer-swimmer hydrodynamic interactions [68].

Therefore, here we analytically study the effects of spatial variation of viscosity on the locomotion velocity of a model crawler, which is a deforming body on a lubricating Newtonian fluid (Fig. 1). Our first aim is to derive a general velocity formula for crawling locomotion with spatial viscosity variations. The second aim of this study is then to examine the emergent nonlinear, multiscale coupling between the surface oscillation and spatial viscosity variation. In doing so, we perform a multiscale perturbation analysis to derive the asymptotic long-term average dynamics, mainly focusing on two important cases with a shape viscosity interface and with a linear viscosity gradient.

This article is organized as follows. In Sec. II, we derive a formula for locomotion velocity on a lubricating fluid [Eq. (27)], which is used thereafter. Also, to deal with a self-deforming object with both longitudinal and transverse traveling waves, we derive useful formulas by small-amplitude expansions. In Sec. III, we start by examining a situation where the fluid viscosity is uniform. We find that the longitudinal and transverse waves correspond to direct and retrograde crawlers, respectively. In Sec. IV, we consider locomotion on a fluid with an abrupt viscosity change (a vis-

TABLE I. Summary of the leading-order average locomotion velocity for the sinusoidal deformation given by Eq. (34).

Viscosity profile	Velocity (transverse wave)	Velocity (longitudinal wave)	Section
Uniform	$U_0^{(y)} = -\frac{3\omega}{h_0^2 k} A_y^2\ (<0)$	$U_0^{(x)} = \frac{k\omega}{2} A_x^2\ (>0)$	III
Jump	$\geqslant U_0^{(y)}$ (speed down)	$\leqslant U_0^{(x)}$ (speed down)	IV
Gradient	$\geqslant U_0^{(y)}$ (speed down)	$\simeq U_0^{(x)}$ (almost the same)	V

cosity "jump") and explicitly derive asymptotic locomotion velocities. Then, we perform multiple timescale analysis to average the velocity over a fast timescale (a period of oscillation of traveling waves) and demonstrate that the locomotion speed is reduced by the viscosity jump [Eqs. (68) and (84)]. In Sec. V, we examine the crawler with a linear viscosity gradient in space. In this situation, through the multiscale analysis, we show that the viscosity gradient decreases the crawling speed for a transverse wave, but the same crawler with a longitudinal wave has almost the same speed even with the viscosity gradient. In Sec. VI, we summarize our main findings and draw conclusions. The asymptotic time-averaged velocities obtained in this study are also summarized in Table I.

II. LOCOMOTION VELOCITY FORMULA

A. Setup

We consider a viscous incompressible Newtonian fluid with position-dependent viscosity μ confined by two boundaries (Fig. 1). The upper boundary is a crawler's body surface, while the lower boundary is a flat and rigid substrate. We assume that the system depends only on x and y, and therefore is invariant in the third direction z. Let $x_1(t)$ and $x_2(t)[>x_1(t)]$ be the ends of the lubricating fluid region, corresponding to the body of a crawler. Thus, the crawler is of finite length in the x direction. We denote the height of the upper boundary (the crawler's body) in the laboratory frame of reference as $h(x, t)$.

In the laboratory frame [Fig. 1(a)], the upper boundary, in general, deforms in both the x and y directions, with the instantaneous velocities denoted by $U(x, t)$ for the tangential (x) components and $V(x, t)$ for the normal (y) components. In the laboratory frame, where the substrate is in rest, the crawler moves along the x axis with velocity $U_0(t)$ and does not move along the y axis. Thus, $U_0(t)$ is an instantaneous locomotion velocity of the crawler. We also introduce a reference frame attached to the upper boundary, termed the crawler frame [Fig. 1(b)]. We denote a surface velocity of the crawler in the crawler frame as $[U^{(c)}(x, t), V^{(c)}(x, t)]^T$,

$$U^{(c)}(x, t) = U(x, t) - U_0(t), \tag{1}$$

$$V^{(c)}(x, t) = V(x, t). \tag{2}$$

The body deformation of a crawler should be defined in the crawler frame, not in the laboratory frame, since the deformation is controlled by the crawler itself.

We denote X and Y as typical length scales in the directions of x and y, respectively, and assume that their ratio is small so that the lubrication approximation is valid, that is, $Y/X \ll 1$. We typically take X as a wavelength of the crawler deformation and Y as the mean height of the crawler from the substrate. From the Navier-Stokes equations, the leading-order equations for the fluid motion are obtained as [69–71]

$$\frac{\partial p}{\partial x} = \frac{\partial}{\partial y}\left(\mu \frac{\partial u}{\partial y}\right), \tag{3}$$

$$\frac{\partial p}{\partial y} = 0, \tag{4}$$

where $\mu(x, y, t)$ is the fluid viscosity, $p(x, y, t)$ is a pressure field, and $u(x, y, t)$ denotes the fluid velocity in the x direction. The fluid viscosity can spatially vary in the presence of inhomogeneous distribution of chemical concentration [40] and temperature [72], which we denote by a general scalar field $c(x, y, t)$ (concentration or temperature field). We then write the viscosity as a function of a general scalar field c such that $\mu = \mu(c(x, y, t))$ and assume that the scalar field follows the advection-diffusion equation,

$$\frac{\partial c}{\partial t} + u\frac{\partial c}{\partial x} + v\frac{\partial c}{\partial y} = D\left(\frac{\partial^2 c}{\partial x^2} + \frac{\partial^2 c}{\partial y^2}\right), \tag{5}$$

where $v(x, y, t)$ is the fluid velocity in the y direction and D is the diffusion constant of the scalar field. To derive the equation in the lubricating situation, we estimate the order of magnitude of both sides of Eq. (5). The ratio between the left- and right-hand sides is then estimated to be at the order of $\mathrm{Pe}(Y/X)$ with the Péclet number $\mathrm{Pe} = \hat{U}Y/D$, where $\hat{U}$ is the characteristic speed of the system. At the leading order of Y/X, we thus have [71]

$$\frac{\partial^2 c}{\partial y^2} = 0, \tag{6}$$

which allows us to neglect the diffusion in the x direction and the advection of the scalar in both x and y directions. If the scalar field has the same value at the bottom and upper surfaces, $c(x, y = 0, t) = c(x, y = h, t) = c_0(x, t)$, we have $c(x, y, t) = c_0(x, t)$ for all y with $0 \leqslant y \leqslant h(x, t)$, indicating that the fluid viscosity $\mu(c(x, y, t))$ is also independent of y. Therefore, we hereafter assume that viscosity μ may depend on position x but not y (i.e., $\partial\mu/\partial y = 0$). Equation (3) then reduces to

$$\frac{\partial p}{\partial x} = \mu\frac{\partial^2 u}{\partial y^2}. \tag{7}$$

From Eq. (7), we find that we can neglect the advection and diffusion in the x direction in the lubrication limit. In the current study, therefore, we consider a fixed viscosity profile $\mu(x)$, which is constant over time.

B. Locomotion velocity of the crawler

Here, we derive a velocity formula that provides a locomotion velocity of the crawler in the laboratory frame, following standard procedures [15], but we generalize to the case with position-dependent viscosity and tangential deformation. Because our working equations [Eqs. (4), (6), and (7)] do not explicitly depend on time t, the state of the system is determined only by instantaneous physical quantities with no history dependence. In addition, from Eq. (4), p is independent of y, that is, $p(x, t)$. Hence, we simply write $\partial p/\partial x$ as dp/dx. Thus, by integrating Eq. (7) twice with respect to y, we obtain

$$u = -\frac{1}{2\mu}\frac{dp}{dx}(h - y)y + \frac{y}{h}U, \tag{8}$$

where we use the no-slip boundary conditions at the fluid boundaries,

$$u = 0 \quad (\text{at} \quad y = 0) \ \text{ and } \ u = U \quad (\text{at} \ \ y = h). \tag{9}$$

The continuity condition ($\nabla \cdot \boldsymbol{u} = 0$) is written as

$$\frac{\partial u}{\partial x} + \frac{\partial v}{\partial y} = 0, \tag{10}$$

where the fluid velocity in the z direction is independent of its position z. Integrating Eq. (10) with respect to y yields

$$0 = \int_0^h \frac{\partial u}{\partial x} dy + [v]_0^h = \frac{d}{dx}\left(\int_0^h u dy\right) - U\frac{dh}{dx} + V. \tag{11}$$

Here, we used no-slip boundary conditions for u [Eq. (9)] and v,

$$v = 0 \quad (\text{at } y = 0) \text{ and } v = V \quad (\text{at } y = h). \tag{12}$$

From Eq. (8), we find

$$\int_0^h u dy = -\frac{h^3}{12\mu}\frac{dp}{dx} + \frac{1}{2}Uh, \tag{13}$$

and thus,

$$\frac{d}{dx}\left(\int_0^h u dy\right) = \frac{d}{dx}\left(-\frac{h^3}{12\mu}\frac{dp}{dx}\right) + \frac{1}{2}U\frac{dh}{dx} + \frac{1}{2}h\frac{dU}{dx}. \tag{14}$$

Plugging Eq. (14) into Eq. (11) and integrating by x, we obtain

$$\frac{dp}{dx} = \frac{\mu}{h^3}[F(x) - C], \tag{15}$$

with

$$F(s) = \int_{x_1}^s 6\left(-U\frac{dh}{dx} + h\frac{dU}{dx} + 2V\right)dx, \tag{16}$$

where C is a constant of integration. We assume that the pressures on both ends are equal,

$$\Delta p = p(x_2) - p(x_1) = 0, \tag{17}$$

because fluid pressures are in balance with ambient pressures (e.g., atmospheric pressures) at the ends. As a side note, this pressure balance [Eq. (17)] also holds for a spatially periodic surface deformation, where the system is invariant under a discrete parallel displacement $x \to x \pm (x_2 - x_1)$. The constant C is then determined by enforcing Eq. (17) as

$$C = \left(\int_{x_1}^{x_2} \frac{\mu F(x)}{h^3} dx\right) \Big/ \left(\int_{x_1}^{x_2} \frac{\mu}{h^3} dx\right). \tag{18}$$

We impose a force balance on the crawler to obtain a locomotion velocity. The force acting on the upper side, $\boldsymbol{f} = (f_x, f_y)^{\mathrm{T}}$, is given by

$$\boldsymbol{f} = \boldsymbol{\sigma} \cdot \boldsymbol{n}, \tag{19}$$

with the fluid stress tensor of Newtonian fluids,

$$\sigma_{ij} = -p\delta_{ij} + \mu\left(\frac{\partial u_i}{\partial x_j} + \frac{\partial u_j}{\partial x_i}\right), \quad i, j \in \{x, y\}, \tag{20}$$

where δ_{ij} is the Kronecker delta and $\boldsymbol{n}$ is the outward unit normal to the upper surface. Under the lubrication approximation, the stress tensor is simply

$$\sigma_{xx} = -p + 2\mu\frac{\partial u}{\partial x} \simeq -p \text{ and } \sigma_{xy} = \mu\left(\frac{\partial u}{\partial y} + \frac{\partial v}{\partial x}\right) \simeq \mu\frac{\partial u}{\partial y}, \tag{21}$$

and the normal vector reduces to

$$\boldsymbol{n} \simeq \left(\frac{dh}{dx}, -1\right)^{\mathrm{T}}. \tag{22}$$

Thus, the force-balance condition in the x direction is read as

$$0 = \int_{x_1}^{x_2} f_x dx = \int_{x_1}^{x_2} (\sigma_{xx}n_x + \sigma_{xy}n_y)|_{y=h} dx \tag{23}$$

$$= [-ph]_{x_1}^{x_2} - \int_{x_1}^{x_2} \left(-h\frac{dp}{dx} + \mu \left.\frac{\partial u}{\partial y}\right|_{y=h}\right) dx \tag{24}$$

$$= -\int_{x_1}^{x_2} \left(-\frac{1}{2}h\frac{dp}{dx} + \mu\frac{U}{h}\right) dx. \tag{25}$$

Here, we perform integration by parts in Eq. (24) and use Eq. (17) and the relation

$$\frac{\partial u}{\partial y} = \frac{1}{2\mu}(2y - h)\frac{dp}{dx} + \frac{U}{h}, \tag{26}$$

which is obtained from Eq. (8) in Eq. (25). We also assume $h(x_1) = h(x_2)$ for simplicity.

By plugging Eqs. (15) and (18) into the force-balance relation [Eq. (25)], we may explicitly determine the locomotion velocity U_0. After some calculations with Eqs. (1) and (2), we obtain

$$U_0 = \frac{-4I[h^2U^{(c)}]I[1] + 3I[hU^{(c)}]I[h] + 6I[hJ(x)]I[1] - 6I[h]I[J(x)]}{4I[h^2]I[1] - 3(I[h])^2}, \tag{27}$$

with

$$I[G(x)] = \int_{x_1}^{x_2} \frac{\mu G(x)}{h^3} dx \tag{28}$$

and

$$J(s) = \int_{x_1}^{s} \left(h\frac{dU^{(c)}}{dx} + V^{(c)}\right) dx. \tag{29}$$

As the x-dependent surface velocities in the crawler frame are $U^{(c)} = U - U_0$ and $V^{(c)} = V$, Eq. (27) provides an instantaneous locomotion velocity for a given fluid viscosity profile and an instantaneous surface shape with its deformation velocity.

Our result [Eq. (27)] is a generalization of known results for the case with spatially dependent viscosity and tangential deformation. For example, when the fluid viscosity is spatially homogeneous and only the normal surface deformation is considered, that is, $d\mu/dx = 0$ and $U^{(c)} = 0$, the expression in Eq. (27) readily recovers the velocity formula of Chan *et al.* [15].

C. Small surface deformation

In the above subsections, we treat h, U, and V as independent variables. However, these variables should be determined by the movement of surface points. Let us introduce a Lagrangian label of a material point on the surface, $\boldsymbol{\xi}$, by the position on an undeformed flat surface in the frame moving together with the surface, that is, $\boldsymbol{\xi} = (\xi, 0)^{\mathrm{T}}$ (Fig. 2). Hereafter, we consider small deformations of the surface for explicit calculations of surface shapes and velocities.

We introduce the positions of the material points after deformation as

$$\boldsymbol{h}(\boldsymbol{\xi}, t) = [h_x(\boldsymbol{\xi}, t), h_y(\boldsymbol{\xi}, t)]^{\mathrm{T}}, \tag{30}$$

and assume the deformation $\boldsymbol{\delta}$ is on the order of ϵ, where $\epsilon \ll 1$ is a small parameter, or explicitly,

$$\boldsymbol{\delta}(\boldsymbol{\xi}, t) = \boldsymbol{h}(\boldsymbol{\xi}, t) - \boldsymbol{\xi} = \begin{pmatrix} h_x(\boldsymbol{\xi}, t) - \xi \\ h_y(\boldsymbol{\xi}, t) \end{pmatrix} = \begin{pmatrix} O(\epsilon) \\ O(\epsilon) \end{pmatrix}. \tag{31}$$

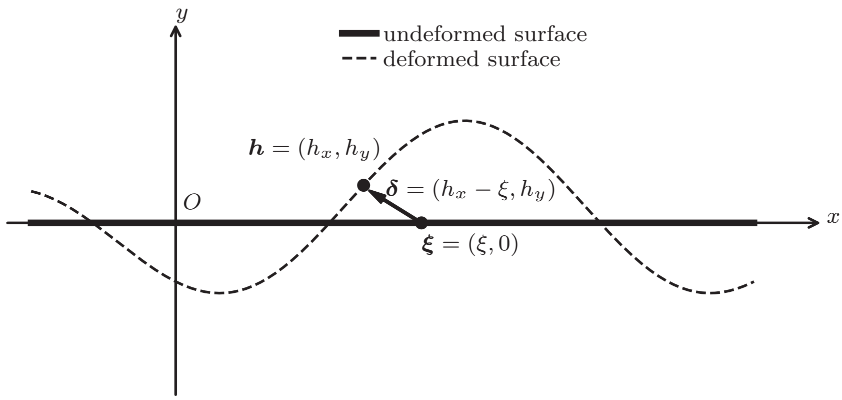

FIG. 2. Schematic of an undeformed flat surface (thick line) and a deformed surface (dashed line). We take the position of an undeformed flat surface, $\boldsymbol{\xi} = (\xi, 0)^{\mathrm{T}}$, in the frame attached to the surface as a Lagrangian label of material points. The surface profile $\boldsymbol{h}$ is given by $\boldsymbol{h} = \boldsymbol{\xi} + \boldsymbol{\delta}$.

From the Taylor expansion, the Eulerian expression of the surface position is obtained as

$$\boldsymbol{h}_{\mathrm{E}}(x,t) = \left.\begin{pmatrix} \xi \\ [1 - (h_x - \xi)\frac{\partial}{\partial \xi}]h_y(\boldsymbol{\xi}, t) \end{pmatrix}\right|_{\boldsymbol{\xi}=(x,0)^{\mathrm{T}},\xi=x} + \begin{pmatrix} O(\epsilon^3) \\ O(\epsilon^3) \end{pmatrix}, \tag{32}$$

where the subscript E denotes the Eulerian expression. Similarly, the velocity vector is given by

$$\boldsymbol{U}_{\mathrm{E}}(x,t) = \left.\left\{\left[1 - (h_x - \xi)\frac{\partial}{\partial \xi}\right]\frac{\partial}{\partial t}\begin{pmatrix} h_x(\boldsymbol{\xi}, t) \\ h_y(\boldsymbol{\xi}, t) \end{pmatrix}\right\}\right|_{\boldsymbol{\xi}=(x,0)^{\mathrm{T}},\xi=x} + \begin{pmatrix} O(\epsilon^3) \\ O(\epsilon^3) \end{pmatrix}. \tag{33}$$

As an illustrative example used hereafter, we consider a combination of sinusoidal waves traveling in the $+x$ direction with oscillation in the x (longitudinal) and y (transverse) directions,

$$\boldsymbol{h}(\boldsymbol{\xi}, t) = \begin{pmatrix} \xi + A_x \sin(k\xi - \omega t) \\ h_0 + A_y \sin(k\xi - \omega t + \phi) \end{pmatrix}, \tag{34}$$

with amplitudes A_x, A_y (>0) being on the order of ϵ and a phase shift ϕ between waves oscillating in the x and y directions. Here, the wavenumber k (>0) and the angular frequency ω (>0) are assumed to be the same for both waves. To give $h_x(\xi; t) = \xi + A_x \sin(k\xi - \omega t)$ its inverse function $\xi(h_x)$, A_x must satisfy $A_x \leqslant 1/k$, which is consistent with the small-amplitude expansion, $A_x = O(\epsilon)$, with $k = 2\pi$ used hereafter. For later use, we calculate $\boldsymbol{h}_{\mathrm{E}}$ and $\boldsymbol{U}_{\mathrm{E}}$ by substituting Eq. (34) into Eqs. (32) and (33) to obtain

$$\boldsymbol{h}_{\mathrm{E}}(x,t) = \begin{pmatrix} x \\ h_0 + A_y \sin(kx - \omega t + \phi) - A_x A_y k \sin(kx - \omega t)\cos(kx - \omega t + \phi) \end{pmatrix} + O(\epsilon^3) \tag{35}$$

and

$$\boldsymbol{U}_{\mathrm{E}}(x,t) = \begin{pmatrix} -A_x\omega\cos(kx - \omega t) - A_x^2\omega k \sin^2(kx - \omega t) \\ -A_y\omega\cos(kx - \omega t + \phi) - A_x A_y \omega k \sin(kx - \omega t)\sin(kx - \omega t + \phi) \end{pmatrix} + O(\epsilon^3). \tag{36}$$

In the subsequent sections, we apply the traveling-wave type deformations [Eqs. (35) and (36)] to the locomotion velocity formula [Eq. (27)] with spatially varying fluid viscosity. In Sec. III, we examine the case with uniform viscosity. We then analyze the cases of abrupt change in viscosity in Sec. IV and linear viscosity gradient in Sec. V. The results of our analysis are summarized in Table I.

III. LOCOMOTION WITH A UNIFORM VISCOSITY

Before proceeding to a detailed analysis of the inhomogeneous viscosity effects on the locomotion speed, here we discuss the case of uniform viscosity. We consider a crawling motion over a thin fluid film with a uniform viscosity by a deformation with a traveling wave given by Eq. (34). The profile of the crawler surface is given as in Eq. (34) in the crawler frame, comoving with the crawler. Then, we can use the results derived in Sec. II C [Eqs. (35) and (36)]. That is,

$$h(x,t) = h_0 + A_y \sin(kx - \omega t + \phi) - A_x A_y k \sin(kx - \omega t)\cos(kx - \omega t + \phi) + O(\epsilon^3), \quad (37)$$

$$U^{(c)}(x,t) = -A_x\omega\cos(kx - \omega t) - A_x^2\omega k \sin^2(kx - \omega t) + O(\epsilon^3), \quad (38)$$

$$V^{(c)}(x,t) = -A_y\omega\cos(kx - \omega t + \phi) - A_x A_y \omega k \sin(kx - \omega t)\sin(kx - \omega t + \phi) + O(\epsilon^3). \quad (39)$$

We assume that length scales in the x and y directions are already rescaled so that the lubrication theory applies. Here, we take the wavelength $\lambda = 2\pi/k$ as a typical length scale of x and the distance between the crawler surface and the substrate h_0 as that of y. Then, we can set $k = 2\pi$ and $h_0 = 1$, for example, but we retain the notation for clarity. Note that A_x and A_y are on the order of ϵ in the rescaled settings, indicating that the wave amplitude in the x direction is large enough compared to that in the y direction so that the lubrication approximation holds in the original (unscaled) configuration. For example, gastropods deform their body surface around 10^{-5} to 10^{-4} m in the longitudinal (x) direction compared with the longitudinal wavelength 10^{-3} m [22], and the transverse amplitude is also known to be sufficiently small [11], allowing for a small-amplitude expansion. However, the measurement accuracy for the transverse amplitude is still controversial [22].

We now proceed to derive the locomotion velocity of a crawler on a fluid with a uniform viscosity. By applying $x_1 = -\lambda/2 = -\pi/k$ and $x_2 = \lambda/2 = \pi/k$ and substituting Eqs. (37)–(39) in Eq. (27), we can obtain the instantaneous locomotion velocity U_0 as

$$U_0 = \frac{k\omega}{2}A_x^2 - \frac{3\omega}{h_0^2 k}A_y^2 - \frac{2\omega}{h_0}A_x A_y \sin\phi + O(\epsilon^4), \quad (40)$$

where we perform the Taylor expansion with respect to ϵ. The velocity of the crawler U_0 is then independent of time (i.e., steady motion) and the (uniform) viscosity μ, with the leading-order contribution being on the order of ϵ^2. Although the direction of traveling waves is taken towards the $+x$ direction [see Eq. (34)], the crawler's locomotion can be in both directions, depending on the surface deformation profile. The leading-order velocities are summarized in Table I.

When the wave is purely transverse (i.e., $A_x = 0$ and $A_y \neq 0$), the locomotion velocity becomes

$$U_0^{(y)} = -\frac{3\omega}{h_0^2 k}A_y^2 \ (<0), \quad (41)$$

which is negative, and the crawler always moves in the $-x$ direction, consistent with the results obtained in Chan *et al.* [15]. This locomotion gait is called retrograde crawling because the direction of the traveling wave ($+x$ direction) is opposite to the direction of crawler locomotion ($-x$ direction).

In contrast, if the wave is purely longitudinal (i.e., $A_x \neq 0$ and $A_y = 0$), we have

$$U_0^{(x)} = \frac{k\omega}{2}A_x^2 \ (>0), \quad (42)$$

and the locomotion speed does not depend on the average height between the surface and the substrate, h_0. In this case, the crawler moves in the same direction as the traveling wave and this locomotion gait is known as direct crawling. The expression in Eq. (42) is identical to the swimming speed of a Taylor sheet with longitudinal deformation [73]. Also, a similar expression was obtained for a model crawler with viscous friction [74]. The correspondences between longitudinal deformation and direct wave, and transversal deformation and retrograde wave, are both consistent with experimental observations [21,75,76].

When the transverse and longitudinal waves coexist (i.e., $A_x \neq 0$ and $A_y \neq 0$), the crawler locomotion can be either direct or retrograde crawling depending on the amplitudes A_x, A_y and their phase shift ϕ [see Eq. (40)]. To further examine this effect, we fix the amplitudes as (A_x, A_y). For a given set of (A_x, A_y), there exists a critical phase shift ϕ_0 such that the locomotion speed vanishes (i.e., $U_0 = 0$),

$$\phi_0 = \arcsin\left(\frac{1}{4}\frac{kh_0A_x}{A_y} - \frac{3}{2}\frac{A_y}{kh_0A_x}\right), \tag{43}$$

if $10 - \sqrt{2} \leqslant kh_0A_x/A_y \leqslant 10 + \sqrt{2}$. Thus, when this condition is satisfied, the crawler locomotion becomes either direct or retrograde only by changing the relative phase of the waves with their amplitudes kept constant.

Before moving to the next section, here we remark on the validity of the small-amplitude expansion. For a pure transverse wave with $A_y = 0.3$, the relative error, $\epsilon_{\rm rel} = |(U_0^{\rm num} - U_0^{\rm asym})/U_0^{\rm num}|$, is calculated as $\epsilon_{\rm rel} \approx 0.18$, where $U_0^{\rm num}$ is the velocity by the direct numerical computation of Eq. (27) and $U_0^{\rm asym}$ is the small-amplitude expansion results provided in Eqs. (41) and (42). This relative error rapidly decreases as $\epsilon_{\rm rel} \approx 0.02$ for $A_y = 0.1$, and we numerically confirmed that the asymptotic relation, $\epsilon_{\rm rel} \sim 2A_y^2$, holds for smaller values of A_y. For a pure longitudinal wave, the amplitude needs to be $A_x \leqslant 1/(2\pi) \approx 0.16$ to prevent the material points from overlapping, and the relative errors are found to be extremely small, such as $\epsilon_{\rm rel} < 10^{-10}$ for $A_x = 0.1$, which suggests that the higher-order terms vanish in the small-amplitude expansion. Indeed, we confirmed by the Taylor expansions that the $O(\epsilon^4)$ term of the locomotion velocity vanishes, being compatible with the Taylor sheet model in the absence of a nearby wall [77], whereas our calculations include the wall effect within the lubrication approximation.

IV. LOCOMOTION WITH A VISCOSITY JUMP

We consider a crawling motion over a sharp viscosity interface (jump) on a flat surface by a deformation with a traveling wave given by Eq. (34) (Fig. 3). The profile of the (upper) crawler surface is given as in Eq. (34) in the crawler frame, comoving with the upper surface (crawler) as in Sec. III. We consider a crawling motion across the viscosity jump whose profile in the laboratory frame is given by

$$\mu(x) = \mu_1 H(-x) + \mu_2 H(x), \tag{44}$$

where $H(z)$ is the Heaviside step function. Hence, $\mu = \mu_1(>0)$ for $x < 0$ and $\mu = \mu_2(>0)$ for $x > 0$, and the viscosity interface is located at $x = 0$. Remember that in the lubrication approximation, the horizontal scale is taken as being much larger than the vertical scale. Hence, the sharp viscosity jump is validated when the spatial scale of the viscosity variation is of the same order of h_0 in the original (unscaled) configuration.

A. Instantaneous velocity and time evolution

We now proceed to derive the locomotion velocity of a crawler across the viscosity jump by using the velocity formula [Eq. (27)] in the crawler frame [Fig. 3(b)], where the viscosity interface is located at $x = x_*$, $\mu(x) = \mu_1 H(x_* - x) + \mu_2 H(x - x_*)$ and the interface moves with an instantaneous velocity $-U_0$ in the x direction. By applying $x_1 = -\lambda/2 = -\pi/k$ and $x_2 = \lambda/2 = \pi/k$ in Eq. (27), we can obtain the instantaneous locomotion velocity U_0 as

$$U_0 = \frac{-4I[h^2U^{(c)}]I[1] + 3I[hU^{(c)}]I[h] + 6I[hJ(x)]I[1] - 6I[h]I[J(x)]}{4I[h^2]I[1] - 3(I[h])^2}, \tag{45}$$

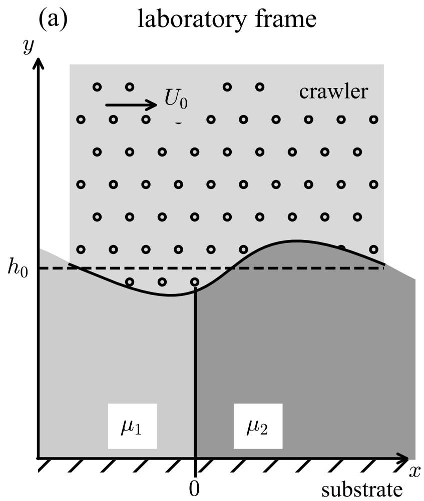

FIG. 3. Schematic of a crawler traveling across a sharp viscosity interface, characterized by the two different viscosity coefficients μ_1 and μ_2 in (a) the laboratory frame and (b) the frame attached to the crawler (crawler frame). (a) In the laboratory frame, the crawler's locomotion velocity is denoted by U_0. (b) In the crawler frame, the viscosity interface, whose position is denoted by x_*, moves with velocity $-U_0$.

with

$$I[G(x)] = \int_{-\lambda/2}^{\lambda/2} \frac{\mu G(x)}{h^3} dx = \mu_1 \int_{-\lambda/2}^{x_*} \frac{G(x)}{h^3} dx + \mu_2 \int_{x_*}^{\lambda/2} \frac{G(x)}{h^3} dx \tag{46}$$

and

$$J(s) = \int_{-\lambda/2}^{s} \left(h \frac{dU^{(c)}}{dx} + V^{(c)} \right) dx. \tag{47}$$

We aim to evaluate U_0 up to the order of ϵ^2. With this in mind, we evaluate each integral by substituting Eqs. (37)–(39). For example, the integral $J(x)$ is on the order of ϵ, and is expanded as

$$J(x) = -h_0 \omega A_x \cos(kx - \omega t) - \frac{\omega}{k} A_y \sin(kx - \omega t + \phi) + \frac{\omega k h_0}{2} A_x^2 \cos 2(kx - \omega t) + C_J + O(\epsilon^3), \tag{48}$$

with

$$C_J = -h_0 \omega A_x \cos(\omega t) + \frac{\omega}{k} A_y \sin(\omega t - \phi) - \frac{\omega k h_0}{2} A_x^2 \cos(2\omega t). \tag{49}$$

By explicit calculations, we find that the viscosity jump generates $O(\epsilon^0)$ contributions at the leading order in $I[1]$, $I[h]$, and $I[h^2]$ as

$$kI[1] = \frac{k(\lambda M/2 + x_* m)}{h_0^3} + \frac{3m}{h_0^4} A_y [\cos(kx_* - \omega t + \phi) - \cos(k\lambda/2 - \omega t + \phi)] + O(\epsilon^2), \tag{50}$$

$$kI[h] = \frac{k(\lambda M/2 + x_* m)}{h_0^2} + \frac{2m}{h_0^3} A_y [\cos(kx_* - \omega t + \phi) - \cos(k\lambda/2 - \omega t + \phi)] + O(\epsilon^2), \tag{51}$$

$$kI[h^2] = \frac{k(\lambda M/2 + x_* m)}{h_0} + \frac{m}{h_0^2} A_y [\cos(kx_* - \omega t + \phi) - \cos(k\lambda/2 - \omega t + \phi)] + O(\epsilon^2), \tag{52}$$

where we introduced

$$m = \mu_1 - \mu_2 \text{ and } M = \mu_1 + \mu_2. \tag{53}$$

The remaining integrals, $I[hU^{(c)}]$, $I[h^2U^{(c)}]$, $I[J(x)]$, and $I[hJ(x)]$, however, have a leading-order contribution on the order of ϵ and need to be expanded up to $O(\epsilon^2)$ for our purpose. Through straightforward but cumbersome Taylor expansions, one may obtain the expression of the instantaneous velocity up to $O(\epsilon^2)$ as

$$\begin{aligned} U_0 = {} & 2\omega A_x K(x_*) \cos\left(\frac{kx_*}{2}\right) \sin\left(\frac{kx_* - 2\omega t}{2}\right) + \frac{k\omega}{2} A_x^2 [1 - K(x_*) \sin(kx_*) \cos(kx_* - 2\omega t)] \\ & - \frac{3\omega}{h_0^2 k} A_y^2 \bigg[1 - K(x_*) \sin(kx_*) \cos(kx_* - 2\omega t + 2\phi) - 8K^2(x_*) \cos^2\left(\frac{kx_*}{2}\right) \\ & \times \cos^2\left(\frac{kx_* - 2\omega t + 2\phi}{2}\right)\bigg] - \frac{2\omega}{h_0} A_x A_y \bigg\{ \sin\phi + K(x_*) \sin(kx_*) \sin(kx_* - 2\omega t + \phi) \\ & - 4K^2(x_*) \cos^2\left(\frac{kx_*}{2}\right) [\sin\phi - \sin(kx_* - 2\omega t + \phi)] \bigg\} + O(\epsilon^3), \end{aligned} \tag{54}$$

where we introduce a nondimensional parameter $K(x_*)$, which is defined as

$$K(x; q) = \frac{q}{k(\lambda/2 + xq)} = \frac{m}{k(\lambda M/2 + xm)}, \tag{55}$$

where $q = m/M = (\mu_1 - \mu_2)/(\mu_1 + \mu_2)$ and $q \in (-1, 1)$ by definition. Note that the velocity U_0 depends on x_* and t, both of which change over time.

When the viscosity interface is located outside the crawler's body (i.e., $x_* \notin [x_1, x_2]$), the crawler's velocity does not depend on the surrounding viscosity, as detailed in Sec. III. Thus, the effects of the viscosity interface on the crawler's velocity are seen only during the time the crawler is crossing the viscosity jump in our lubrication setup. In the crawler frame, the viscosity interface moves with an instantaneous velocity $-U_0$ in the x direction. Therefore, the time evolution of the viscosity interface in the crawler frame is written as

$$\frac{dx_*}{dt} = -U_0(x_*, t). \tag{56}$$

Integrating over time t for some duration t_0, we can formally write an average velocity of the crawler $\overline{U}_0$ as

$$\overline{U}_0 = \frac{1}{t_0} \int_{t'}^{t'+t_0} U_0(x_*(t), t) dt = -\frac{1}{t_0} \int_{t'}^{t'+t_0} \frac{dx_*}{dt} dt = -\frac{x_*(t' + t_0) - x_*(t')}{t_0}. \tag{57}$$

Nonetheless, due to the nonlinear x_* dependence in U_0 [see Eq. (54)], the integration is no longer straightforward.

In Sec. IV B, we analyze the nonlinear effects in the average velocity by exploiting the timescale separation between the crawler's deformation and the locomotion.

B. Multiple timescale analysis

In this subsection, we explore the impact of the viscosity jump on the crawler's locomotion by further analyzing the nonlinear effects in Eq. (54). We first note that there are two timescales in the system: the timescale of the crawler's surface deformation, $\tau_{\text{osc}} = O(1/\omega)$, and the duration of time for the crawler crossing the interface, $\tau_{\text{dur}} = O(\lambda/\overline{U}_0)$, where $\overline{U}_0$ is the average locomotion speed. Moreover, these two timescales are sufficiently separated in our asymptotic regime, because $\tau_{\text{dur}}/\tau_{\text{osc}} = O(1/\epsilon^2)$, as we will see below.

Our focus is therefore on the crawler's long-term behavior after averaging out the rapid oscillation of self-deformation. To do so, we exploit the multiple timescale analysis (e.g., Walker *et al.* [63]) and introduce the fast time variable $T = \omega t$ with $\omega \gg 1$, where t denotes the slow time variable.

Below, we focus on two representative cases with the pure transverse wave ($A_x = 0$ and $A_y \neq 0$) and the pure longitudinal wave ($A_x \neq 0$ and $A_y = 0$).

1. Case of transverse wave (retrograde crawler)

We start with the transverse wave case with $A_x = 0$ and $A_y \neq 0$. The locomotion velocity [Eq. (54)] together with Eq. (56) gives

$$\frac{dx_*}{dt} = -U_0^{(y)}\left\{1 - K(x_*)\sin(kx_*)\cos(kx_* - 2\omega t) - 4K^2(x_*)\cos^2\left(\frac{kx_*}{2}\right)[1 + \cos(kx_* - 2\omega t)]\right\}, \tag{58}$$

where $U_0^{(y)} = -3\omega A_y^2/(h_0^2 k)(< 0)$ is the velocity in the absence of the viscosity jump [see Eq. (41)] and we set $\phi = 0$ without loss of generality. Following Walker *et al.* [63], we introduce the formal transformations,

$$t \mapsto (t,\ T),\ x_*(t) \mapsto x_*(t,\ T),\ \text{and}\ \frac{d}{dt} \mapsto \frac{\partial}{\partial t} + \omega\frac{\partial}{\partial T}, \tag{59}$$

and we have the partial differential equation,

$$\frac{\partial x_*}{\partial t} + \omega\frac{\partial x_*}{\partial T} = -U_0^{(y)}\left\{1 - K(x_*)\sin(kx_*)\cos(kx_* - 2T) - 4K^2(x_*)\cos^2\left(\frac{kx_*}{2}\right)[1 + \cos(kx_* - 2T)]\right\}. \tag{60}$$

We then expand x_* by a series of $1/\omega \ll 1$ as

$$x_*(t, T) = x_0(t, T) + \frac{1}{\omega}x_1(t, T) + \frac{1}{\omega^2}x_2(t, T) + \cdots. \tag{61}$$

The left side of Eq. (60) becomes

$$\frac{\partial x_*}{\partial t} + \omega\frac{\partial x_*}{\partial T} = \omega\frac{\partial x_0}{\partial T} + \left(\frac{\partial x_0}{\partial t} + \frac{\partial x_1}{\partial T}\right) + \frac{1}{\omega}\left(\frac{\partial x_1}{\partial t} + \frac{\partial x_2}{\partial T}\right) + O(\omega^{-2}), \tag{62}$$

while the right side of Eq. (60) is $O(\omega^0)$. Thus, the leading-order contribution is the $O(\omega)$ term, and we have

$$\frac{\partial x_0}{\partial T} = 0. \tag{63}$$

This indicates that x_0 is a function of t only, i.e., $x_0(t, T) = \bar{x}_0(t)$. The subleading $O(\omega^0)$ term is then written as

$$\frac{d\bar{x}_0}{dt} + \frac{\partial x_1}{\partial T} = -U_0^{(y)}\left\{1 - K(\bar{x}_0)\sin(k\bar{x}_0)\cos(k\bar{x}_0 - 2T) - 4K^2(\bar{x}_0)\cos^2\left(\frac{k\bar{x}_0}{2}\right)[1 + \cos(k\bar{x}_0 - 2T)]\right\}. \tag{64}$$

Here, we impose the solvability condition

$$\left\langle\frac{\partial x_1}{\partial T}\right\rangle = 0, \tag{65}$$

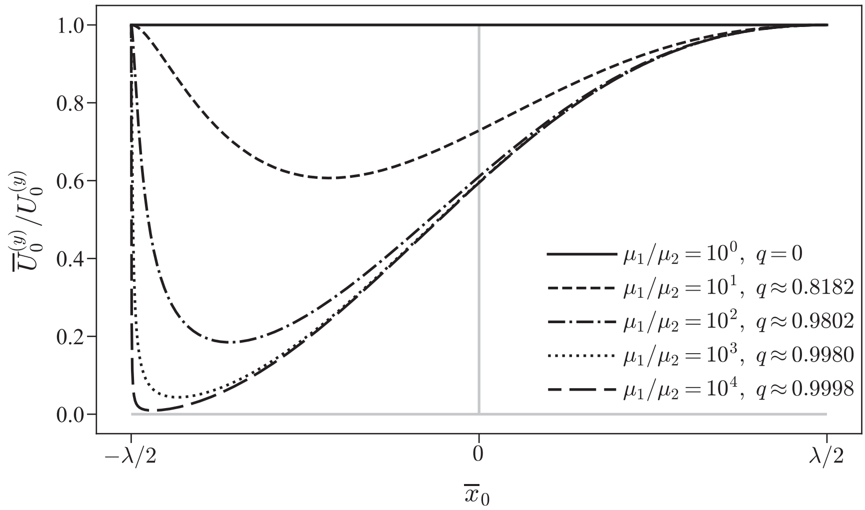

FIG. 4. Reduction in locomotion velocity caused by a viscosity jump. The ratio of the locomotion velocities with and without a viscosity interface, $\overline{U}_0^{(y)}/U_0^{(y)}$ [see Eq. (68)], is plotted as a function of $\bar{x}_0$ for selected values of viscosity ratios and values of q. We set $k = 2\pi$ and $\lambda = 1$.

with $\langle f \rangle$ denoting the time average of a function f over a period of fast timescale T,

$$\langle f \rangle = \frac{1}{2\pi}\int_0^{2\pi} f(t, T)dT. \tag{66}$$

By taking an average over T of both sides of Eq. (64), we find

$$\frac{d\bar{x}_0}{dt} = -U_0^{(y)}\left[1 - 4K^2(\bar{x}_0)\cos^2\left(\frac{k\bar{x}_0}{2}\right)\right], \tag{67}$$

by $\langle \cos(k\bar{x}_0 - 2T)\rangle = 0$. We note that q ranges in $q \in (-1, 1)$, $\bar{x}_0 \in [-\lambda/2, \lambda/2]$, and $k\lambda = 2\pi$; thus, the quantity in $[\dots]$ in the right side of Eq. (67) is strictly positive (see Fig. 4). Hence, by $U_0^{(y)} < 0$, the leading-order effective velocity averaged over the fast timescale, $\overline{U}_0^{(y)}$, given by

$$\overline{U}_0^{(y)} = U_0^{(y)}\left[1 - 4K^2(\bar{x}_0)\cos^2\left(\frac{k\bar{x}_0}{2}\right)\right], \tag{68}$$

is negative definite, and we find that the effective locomotion speed is lower than that in the uniform viscosity environment, that is, $|\overline{U}_0^{(y)}| \leqslant |U_0^{(y)}|$. Equation (68) also shows that the two timescales introduced in the beginning of this subsection are sufficiently separated, $\tau_{\mathrm{dur}}/\tau_{\mathrm{osc}} = O(\omega\lambda/\overline{U}_0) = O(1/\epsilon^2)$.

Therefore, if the crawler has only a transverse traveling wave on its surface, the viscosity jump suppresses the locomotion speed as it crosses the interface. Moreover, this speed reduction occurs irrespective of the direction of travel (i.e., the sign of m or q). The decrease of the locomotion speed is characterized by $|q|$, which is made clear by noting that the locomotion velocity [Eq. (67)] is invariant under the transformations of $q \mapsto -q$, $\bar{x}_0 \mapsto -\bar{x}_0$, and $t \mapsto -t$.

In Fig. 4, we plot $\overline{U}_0^{(y)}/U_0^{(y)}$ in Eq. (68) as a function of $\bar{x}_0$ for different values of $q(\geqslant 0)$, corresponding to the viscosity difference ratio, $\mu_1/\mu_2 \in \{10^0, 10^1, \dots, 10^4\}$. Note that the right side of Eq. (68) is invariant under the transformations $\bar{x}_0 \mapsto -\bar{x}_0$ and $q \mapsto -q$. Further, by analyzing the value of Eq. (68), we find that the speed decrease becomes remarkable when the crawler's front penetrates the high-viscosity layer or when the crawler's rear exits from the high-viscosity

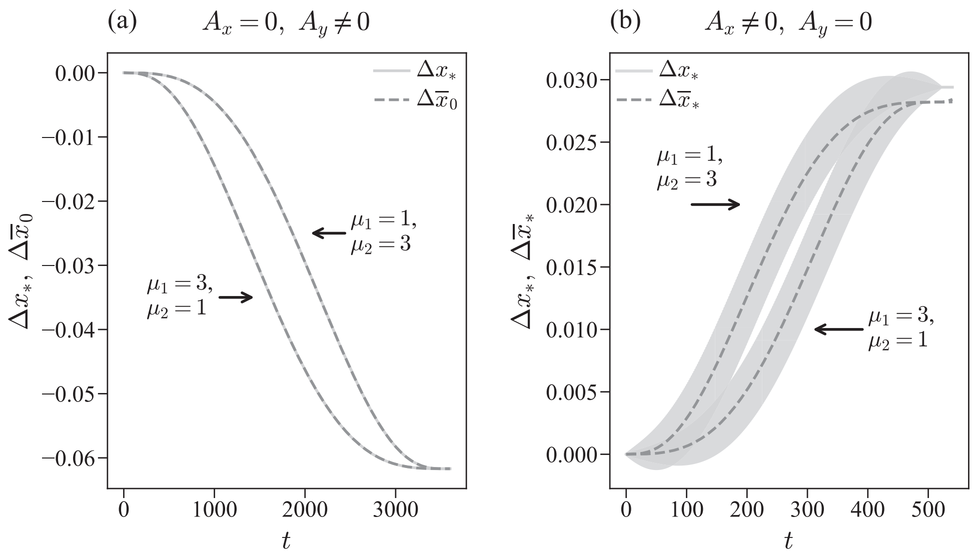

FIG. 5. Results of numerical simulation with a viscosity jump for (a) a transverse wave and (b) a longitudinal wave. The time evolution of the deviations of the position from the locomotion without a viscosity jump, Δx_* (solid lines; without averaging) and $\Delta \bar{x}_0$ or $\Delta \bar{x}_*$ (dashed lines; with averaging), is shown. See the main text for definitions [Eqs. (69) and (70) for (a) and Eqs. (85) and (86) for (b)]. The thickness of the solid lines represents the range of Δx_*. Parameters are $\mu_i = 1, 3$ for $i \in \{1, 2\}$ and thus $q = \pm 1/2$, $A_j = 0, 0.01$ for $j \in \{x, y\}$, $\lambda = 1$, $k = 2\pi$, $\omega = 2\pi$, and $h_0 = 1$. We show the time evolution over the whole period when the crawler crosses over the viscosity jump.

layer. Moreover, the amount of speed drop monotonically increases as the viscosity difference $|q|$ increases.

To further validate our asymptotic analysis for the slow timescale, we calculate time evolution of x_*. In Fig. 5(a), we compare the results of numerical simulation of the fast and slow timescale dynamics. For visualization, we subtract a motion under the uniform viscosity and plot the time evolutions of

$$\Delta x_* = x_* + U_0^{(y)} t \tag{69}$$

for the fast timescale dynamics and

$$\Delta \bar{x}_0 = \bar{x}_0 + U_0^{(y)} t \tag{70}$$

for the time-averaged slow dynamics. As shown in the figure, the asymptotic multiscale analysis clearly captures the average behavior. Note that Δx_* oscillates but its amplitude is so small that it falls within the solid line. From the symmetry in Eq. (67), the changes of $\mu_1 \leftrightarrow \mu_2$ (i.e., $q \mapsto -q$) do not alter the total duration of time needed to travel across the interface, as shown in Fig. 5(a).

2. *Case of longitudinal wave (direct crawler)*

We now consider locomotion with a longitudinal surface wave with $A_x \neq 0$ and $A_y = 0$. As seen in Eq. (54), the leading-order oscillation term is of $O(\epsilon)$, being distinct from the transverse wave case, where the leading order is of $O(\epsilon^2)$. The leading-order contribution in the locomotion velocity [Eq. (56)] is then written as

$$\frac{dx_*}{dt} = -U_0^{(x)} - BK(x_*) \cos\left(\frac{kx_*}{2}\right) \sin\left(\frac{kx_* - 2T}{2}\right), \tag{71}$$

where $U_0^{(x)} = k\omega A_x^2/2(>0)$ is the velocity with uniform viscosity in Eq. (42), and $B = 2\omega A_x(>0)$ is a positive constant. Here, we dropped the subleading correction term of $O(\epsilon^2)$.

Now, we proceed to examine the nonlinear effects of the viscosity jump by multiple timescale analysis as in the previous subsection. By the formal transformation [Eq. (59)] and series expansion with respect to ω^{-1} [Eq. (61)], the $O(\omega)$ term is simply $\partial x_0/\partial T = 0$, and thus we have $x_0(t, T) = \bar{x}_0(t)$. Similarly, the $O(\omega^0)$ term is written as

$$\frac{d\bar{x}_0}{dt} + \frac{\partial x_1}{\partial T} = -U_0^{(x)} - BK(\bar{x}_0)\cos\left(\frac{k\bar{x}_0}{2}\right)\sin\left(\frac{k\bar{x}_0 - 2T}{2}\right). \tag{72}$$

By taking the average over the fast timescale T with the solvability condition $\langle\partial x_1/\partial T\rangle = 0$, we find

$$\frac{d\bar{x}_0}{dt} = -U_0^{(x)} \tag{73}$$

from $\langle\sin(k\bar{x}_0/2 - T)\rangle = 0$. Integration over the slow timescale t yields

$$\bar{x}_0 = \frac{\lambda}{2} - U_0^{(x)}t \tag{74}$$

with an initial condition $\bar{x}_0(0) = \lambda/2$. Equation (74) is exactly the same as the case without a viscosity jump. To obtain the nonzero effects, we need to proceed to the next order.

Substituting Eq. (73) into Eq. (72) and integrating it by the fast timescale T, we have

$$x_1(t, T) = E(t, T) - \langle E\rangle + \bar{x}_1(t), \tag{75}$$

where $E(t, T)$ is given by

$$\begin{aligned} E(t, T) = \int_0^T \Bigg[& -BK(\bar{x}_0)\cos\left(\frac{k\bar{x}_0}{2}\right)\sin\left(\frac{k\bar{x}_0 - 2T'}{2}\right) \\ & - \left\langle -BK(\bar{x}_0)\cos\left(\frac{k\bar{x}_0}{2}\right)\sin\left(\frac{k\bar{x}_0 - 2T}{2}\right)\right\rangle\Bigg|_{T=T'}\Bigg]dT', \end{aligned} \tag{76}$$

or explicitly,

$$E(t, T) = -BK(\bar{x}_0)\cos\left(\frac{k\bar{x}_0}{2}\right)\left[\cos\left(\frac{k\bar{x}_0 - 2T}{2}\right) - \cos\left(\frac{k\bar{x}_0}{2}\right)\right]. \tag{77}$$

The $O(\omega^{-1})$ term in the expansion is then summarized as

$$\frac{\partial x_1}{\partial t} + \frac{\partial x_2}{\partial T} = BK(\bar{x}_0)kx_1\left[K(\bar{x}_0)\cos\left(\frac{k\bar{x}_0}{2}\right)\sin\left(\frac{k\bar{x}_0 - 2T}{2}\right) - \frac{1}{2}\cos(k\bar{x}_0 - T)\right]. \tag{78}$$

We now repeat the same procedure to obtain the slow timescale dynamics by averaging over the fast timescale with the solvability condition, $\langle\partial x_2/\partial T\rangle = 0$, as

$$\left\langle\frac{\partial x_1}{\partial t}\right\rangle = \left\langle BK(\bar{x}_0)kE(t, T)\left[K(\bar{x}_0)\cos\left(\frac{k\bar{x}_0}{2}\right)\sin\left(\frac{k\bar{x}_0 - 2T}{2}\right) - \frac{1}{2}\cos(k\bar{x}_0 - T)\right]\right\rangle, \tag{79}$$

where we substitute Eq. (75) and use the relations $\langle\sin(k\bar{x}_0/2 - T)\rangle = \langle\cos(k\bar{x}_0 - T)\rangle = 0$. We then continue to calculate the average with Eq. (77), using some trigonometric identities, $\langle\sin(k\bar{x}_0/2 - T)\rangle = \langle\cos(k\bar{x}_0 - T)\rangle = \langle\sin(k\bar{x}_0 - 2T)\rangle = \langle\cos(3k\bar{x}_0/2 - T)\rangle = 0$, and the relation

$$\left\langle\frac{\partial x_1}{\partial t}\right\rangle = \frac{\partial}{\partial t}[\langle E(t, T) - \langle E\rangle + \bar{x}_1(t)\rangle] = \frac{d\bar{x}_1}{dt} \tag{80}$$

from Eq. (75). The nonzero effect in the locomotion velocity is then obtained as

$$\frac{d\bar{x}_1}{dt} = k\left[\frac{B}{2}K(\bar{x}_0)\cos\left(\frac{k\bar{x}_0}{2}\right)\right]^2. \tag{81}$$

Note that $d\bar{x}_1/dt$ is on the order of $O(\epsilon^2)$ and is comparable to $U_0^{(x)}$. From Eq. (81), we find $\bar{x}_1 \geqslant 0$ because $\bar{x}_1(0) = 0$ from the initial condition.

Because the slow dynamics of $\bar{x}_*$ has the expansion

$$\bar{x}_* = \bar{x}_0 + \frac{1}{\omega}\bar{x}_1 + O(\omega^{-2}), \tag{82}$$

the time-averaged locomotion velocity $\overline{U}_0^{(x)}$ is obtained as

$$\overline{U}_0^{(x)} = -\frac{d\bar{x}_*}{dt} = U_0^{(x)} - \frac{1}{\omega}\frac{d\bar{x}_1}{dt} + O(\omega^{-2}) \leqslant U_0^{(x)}. \tag{83}$$

The leading-order term is therefore given by

$$\overline{U}_0^{(x)} = U_0^{(x)}\left[1 - 2K^2(\bar{x}_0)\cos^2\left(\frac{k\bar{x}_0}{2}\right)\right]. \tag{84}$$

Remarkably, the correction term in Eq. (84) has the same form as in the transverse case [Eq. (68)]. Hence, we can draw the same conclusion on the crawler's velocity except for the overall sign difference: the speed decreases as it crosses the viscosity interface, that is, $0 < \overline{U}_0^{(x)} \leqslant U_0^{(x)}$.

In Fig. 5(b), we compare the fast timescale dynamics and the asymptotic slow dynamics of the viscosity interface in the crawler frame, by plotting the deviations from the locomotion in the absence of a viscosity jump,

$$\Delta x_* = x_* + U_0^{(x)}t \tag{85}$$

for the fast timescale solution and

$$\Delta\bar{x}_* = \bar{x}_0 + \frac{1}{\omega}\bar{x}_1 + U_0^{(x)}t = \frac{1}{\omega}\bar{x}_1 \tag{86}$$

for the slow timescale solution. As in the figure, both numerical results clearly agree. The final deviation distance is invariant under the change of $\mu_1 \leftrightarrow \mu_2$ (i.e., $q \mapsto -q$), as in the transverse wave case (Sec. IV B 1). As the oscillating terms are $O(\epsilon^2)$ for Fig. 5(a) and $O(\epsilon)$ for Fig. 5(b), oscillation is more evident in Fig. 5(b), as seen in the oscillatory amplitudes of the gray solid lines in Figs. 5(a) and 5(b).

To sum up our analysis up to this point, through multiple timescale analysis we find that the nonlinear coupling between the fast oscillation of the crawler's deformation and the viscosity jump leads to a decrease in the locomotion speed for both transverse and longitudinal waves. In particular, for a longitudinal wave, the effects of the viscosity jump only appear in the higher-order contribution in the multiscale expansion. As a result, for both transverse and longitudinal waves, the average locomotion speed is on the order of $O(\epsilon^2)$ while the fast timescale dynamics contain the $O(\epsilon)$ contribution for the longitudinal wave case.

V. LOCOMOTION WITH A CONSTANT VISCOSITY GRADIENT

In the previous section, we considered locomotion with a sharp viscosity change in the position-dependent viscosity $\mu(x)$, which was represented by a step function [Eq. (44)]. In this section, we discuss the opposite scenario of a gentle change in the viscosity profile, where $\mu(x)$ is a linear function of x (Fig. 6), namely,

$$\mu(x) = \mu_0 + \frac{\gamma x}{\lambda}\ (>0) \tag{87}$$

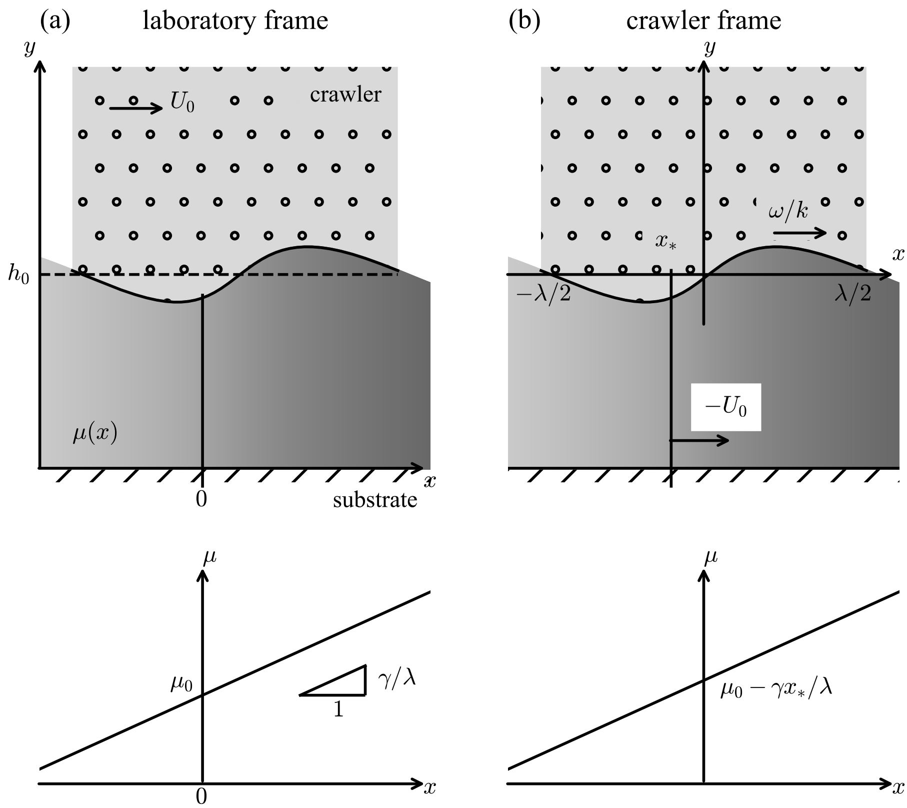

FIG. 6. Schematic of a crawler traveling over a viscosity gradient (top panels), and the viscosity profile, $\mu(x)$ (bottom panels) in (a) the laboratory frame and (b) the frame attached to the crawler (crawler frame). (a) In the laboratory frame, the crawler's locomotion velocity is denoted by U_0. The viscosity linearly depends on the position x, $\mu(x) = \mu_0 + \gamma x/\lambda$ with a constant γ. (b) In the crawler frame, the origin of the laboratory frame, denoted by x_*, moves with an instantaneous velocity $-U_0$.

in the laboratory frame. Here, μ_0 denotes the viscosity at $x = 0$ and γ is a constant slope in the laboratory frame.

As in Secs. III and IV, we consider the same traveling wave profile for the crawler surface, that is, Eq. (34). Hence, the instantaneous locomotion velocity U_0 has the same form as Eq. (45),

$$U_0 = \frac{-4I[h^2U^{(c)}]I[1] + 3I[hU^{(c)}]I[h] + 6I[hJ(x)]I[1] - 6I[h]I[J(x)]}{4I[h^2]I[1] - 3(I[h])^2}, \tag{88}$$

where the expressions of $h(x,t)$, $U^{(c)}(x,t)$, and $V^{(c)}(x,t)$ are provided in Eqs. (37)–(39). The function $I[G(x)]$ now reads as

$$I[G(x)] = \int_{-\lambda/2}^{\lambda/2} \frac{\mu G(x)}{h^3} dx = \mu_* \int_{-\lambda/2}^{\lambda/2} \frac{G(x)}{h^3} dx + \frac{\gamma}{\lambda} \int_{-\lambda/2}^{\lambda/2} \frac{xG(x)}{h^3} dx, \tag{89}$$

while $J(s)$ has the same form as in Eq. (47). To express the crawler position, we introduce the position of the origin of the laboratory frame in the crawler frame as x_* (Fig. 6) and denote the viscosity at the origin of the crawler frame (i.e., the midpoint of the crawler) as μ_*,

$$\mu_*(x_*) = \mu_0 - \frac{\gamma x_*}{\lambda}. \tag{90}$$

We then proceed to the Taylor expansions with respect to small parameters, A_x and A_y, while we assume that the nondimensional function of x_*,

$$D(x_*) = \frac{\gamma x_*}{\mu_0 \lambda}, \tag{91}$$

is not necessarily a small value. By introducing a nondimensional parameter, $\eta(x) = O(\epsilon^0)$, as

$$\eta(x_*) = \frac{\gamma}{k\lambda\mu_*(x_*)} = \frac{\gamma}{k\lambda\mu_0[1 - D(x_*)]}, \tag{92}$$

and performing the Taylor expansions of Eq. (88) with respect to A_x and A_y, we finally obtain

$$U_0 = \omega A_x \eta \sin(\omega t) + \frac{k\omega}{2} A_x^2 \left[1 + \frac{\eta}{2} \sin(2\omega t)\right] - \frac{3\omega}{h_0^2 k} A_y^2 \left[1 + \frac{\eta}{2} \sin 2(\omega t - \phi) - 2\eta^2 \cos^2(\omega t - \phi)\right]$$
$$- \frac{2\omega}{h_0} A_x A_y \left[\sin\phi - \frac{\eta}{2} \cos(2\omega t - \phi) - 2\eta^2 \sin(\omega t) \cos(\omega t - \phi)\right] + O(\epsilon^3). \tag{93}$$

Because x_* is a position of the origin of the laboratory frame in the crawler frame, the rate of change in x_* is $-U_0$, and hence,

$$\frac{dx_*}{dt} = -U_0, \tag{94}$$

as in Eq. (56). In other words, the crawler's representative position in the laboratory frame, $-x_*$, moves with the locomotion velocity U_0. Below, we evaluate the effects of the viscosity gradient on the time-averaged velocity by the multiple timescale analysis as in Sec. IV B.

A. Case of transverse wave (retrograde crawler)

We start with the transverse wave case with $A_x = 0$ and $A_y \neq 0$, corresponding to the retrograde crawler (i.e., $U_0^{(y)} < 0$). By setting $\phi = 0$ without loss of generality, together with the instantaneous velocity [Eq. (93)], we write the equation of motion [Eq. (94)] as

$$\frac{dx_*}{dt} = -U_0^{(y)} \left\{1 + \frac{\eta(x_*)}{2} \sin(2\omega t) - \eta^2(x_*)[1 + \cos(2\omega t)]\right\}, \tag{95}$$

where $U_0^{(y)}$ is the locomotion velocity in the absence of the viscosity gradient [Eq. (41)].

Following the procedures of the multiple timescale analysis [Eqs. (59), (61), and (62)], we first obtain the leading-order dynamics on the order of ω as $\partial x_0/\partial T = 0$, yielding $x_0(t, T) = \bar{x}_0(t)$, where t and $T = \omega t$ are slow and fast timescales, respectively. From the $O(\omega^0)$ contributions of the multiple timescale expansion for Eq. (95) and the solvability condition, $\langle \partial x_1/\partial T\rangle = 0$, we readily find the leading-order slow dynamics,

$$\frac{d\bar{x}_0}{dt} = \left\langle -U_0^{(y)} \left\{1 + \frac{\eta(\bar{x}_0)}{2} \sin(2T) - \eta^2(\bar{x}_0)[1 + \cos(2T)]\right\}\right\rangle = -U_0^{(y)}[1 - \eta^2(\bar{x}_0)]. \tag{96}$$

Therefore, the time-averaged velocity $\overline{U}_0$ follows as

$$\overline{U}_0^{(y)} = U_0^{(y)}[1 - \eta^2(\bar{x}_0)], \tag{97}$$

which indicates that the crawler's locomotion speed decreases by the viscosity gradient, regardless of its gradient direction. The results are similar to those obtained in Sec. IV B 1.

To demonstrate the validity of the multiscale analysis, we show the results of numerical calculation in Fig. 7(a) by plotting position deviations from the locomotion in the absence of a viscosity

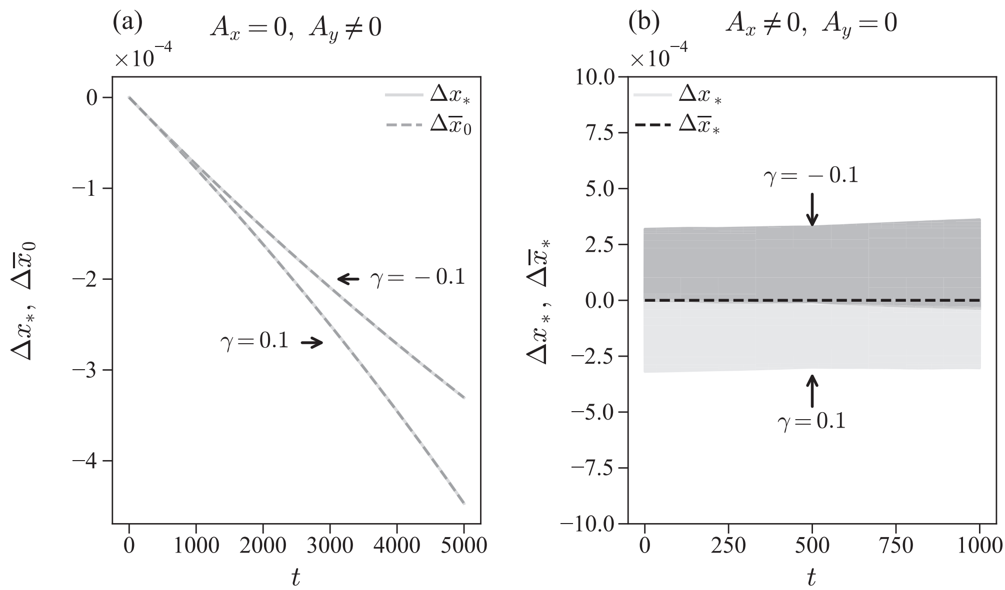

FIG. 7. Results of numerical simulation with a viscosity gradient for (a) a transverse wave and (b) a longitudinal wave. The plots show the time evolution of the deviation of the position from the locomotion without a viscosity gradient, Δx_* (solid lines; without averaging) and $\Delta \overline{x}_0$ or $\Delta \overline{x}_*$ (dashed lines; with averaging). See the main text for definitions [Eqs. (98) and (99) for (a) and Eqs. (110) and (111) for (b)]. The thickness of the solid lines represents the range of Δx_*. Parameters are set as $\mu_0 = 1$, $\gamma = \pm 0.1$ [light gray and dark gray, respectively, in (b)], $\lambda = 1$, $k = 2\pi$, $\omega = 2\pi$, $h_0 = 1$, and $x_*(0) = 0$.

gradient,

$$\Delta x_* = x_* + U_0^{(y)} t \tag{98}$$

for the fast timescale dynamics and

$$\Delta \overline{x}_0 = \overline{x}_0 + U_0^{(y)} t \tag{99}$$

for the averaged slow dynamics. The figure clearly shows that the multiscale analysis captures the average locomotion behavior.

B. Case of longitudinal wave (direct crawler)

We then consider the longitudinal wave case with $A_x \neq 0$ and $A_y = 0$, corresponding to a direct crawler. From Eq. (93), the locomotion velocity in a viscosity gradient is written as

$$U_0 = \omega A_x \eta(x_*) \sin(\omega t) + \frac{k\omega}{2} A_x^2 \left[1 + \frac{\eta(x_*)}{2} \sin(2\omega t) \right]. \tag{100}$$

We then obtain an ordinary differential equation that governs the position of the crawler,

$$\frac{dx_*}{dt} = -U_0^{(x)} - \frac{\eta(x_*)}{2} \left[B \sin T + U_0^{(x)} \sin(2T) \right], \tag{101}$$

where $T = \omega t$ is the fast timescale, $B = 2\omega A_x = O(\epsilon)$, and $U_0^{(x)} = k\omega A_x^2/2 = O(\epsilon^2)$ is the locomotion velocity in the absence of a viscosity gradient [Eq. (42)]. By employing the multiple timescale analysis as in Sec. IV B 2, we first obtain $\partial x_0/\partial T = 0$ as the leading-order fast time dynamics of

$O(\omega)$, and thus $x_0(t,T)=\bar{x}_0(t)$. On the next order, $O(\omega^0)$, we find

$$\frac{d\bar{x}_0}{dt}+\frac{\partial x_1}{\partial T}=-U_0^{(x)}-\frac{\eta(\bar{x}_0)}{2}\big[B\sin T+U_0^{(x)}\sin{(2T)}\big], \tag{102}$$

and by averaging over T with $\langle\partial x_1/\partial T\rangle=0$, we have

$$\frac{d\bar{x}_0}{dt}=-U_0^{(x)}. \tag{103}$$

Thus, no viscosity gradient effect is found, and we proceed to the next order of ω^{-1}. By substituting Eq. (103) into Eq. (102), we can write

$$x_1(t,T)=F(t,T)-\langle F\rangle+\bar{x}_1(t) \tag{104}$$

with

$$\begin{aligned}F(t,T)=\int_0^T&\left\{-\frac{\eta(\bar{x}_0)}{2}\big[B\sin T'+U_0^{(x)}\sin{(2T')}\big]\right.\\&\left.-\left.\left\langle-\frac{\eta(\bar{x}_0)}{2}\big[B\sin T+U_0^{(x)}\sin{(2T)}\big]\right\rangle\right|_{T=T'}\right\}dT',\end{aligned} \tag{105}$$

or explicitly,

$$F(t,T)=\frac{\eta(\bar{x}_0)}{2}\left\{B(\cos T-1)+\frac{U_0^{(x)}}{2}[\cos{(2T)}-1]\right\}. \tag{106}$$

By examining the $O(\omega^{-1})$ terms in Eq. (101), we find

$$\frac{\partial x_1}{\partial t}+\frac{\partial x_2}{\partial T}=-\frac{kx_1}{2}\eta^2(\bar{x}_0)\big[B\sin T+U_0^{(x)}\sin{(2T)}\big]. \tag{107}$$

By substituting Eqs. (104) and (106) into Eq. (107) and averaging over T with $\langle\partial x_2/\partial T\rangle=0$, we obtain

$$\frac{d\bar{x}_1}{dt}=0. \tag{108}$$

Contrary to the case of a sharp viscosity jump described in Sec. IV B 2, the subleading term x_1 vanishes in the slow timescale; in other words, $\bar{x}_1=0$ from the initial condition $\bar{x}_1(0)=0$. Hence, the time-averaged velocity, $\overline{U}_0$, becomes

$$\overline{U}_0^{(x)}=U_0^{(x)}+O(\omega^{-2}). \tag{109}$$

Note the difference in oscillation terms $\cos{(kx_*/2)}\sin{(kx_*/2-T)}$ and $\sin T$ in Eqs. (71) and (101), respectively. Due to the slow modulation of oscillation in Eq. (71), we obtained the nonzero subleading-order effect in the presence of viscosity interface in Sec. IV B 2.

Numerical demonstrations of these multiscale analyses are shown in Fig. 7(b). Similar to the previous sections, we plot the difference in positions between a uniform viscosity and a viscosity with a gradient, defined as

$$\Delta x_*=x_*+U_0^{(x)}t, \tag{110}$$

where x_* is the solution of Eq. (101) for the fast timescale solution, and the results of our multiscale analysis,

$$\Delta\bar{x}_*=\bar{x}_0+\frac{1}{\omega}\bar{x}_1+U_0^{(x)}t=0. \tag{111}$$

In Fig. 7(b), we use $\gamma=\pm0.1$, and we confirm that the average position of $\Delta\bar{x}_*$ is almost constant, although its value is slightly negative (when $\gamma=0.1$) or positive (when $\gamma=-0.1$). This slight difference is due to the initial condition, $h_x(\boldsymbol{\xi}, t = 0) = \xi + A_x \sin(k\xi)$ [Eq. (34)]. Indeed, if we allow h_x to have a different initial phase [i.e., $h_x(\boldsymbol{\xi}, t) = \xi + A_x \sin(k\xi - \omega t + \varphi_0)$ with φ_0 constant], the trend seen in the figure can be reversed depending on the value of φ_0. In other words, $\bar{x}_0$ has a constant of integration, which is determined from the initial condition in the slow timescale dynamics.

In this section, we analyze the case where the viscosity linearly depends on the position x. Through multiple timescale analysis as in the previous section, we find a locomotion speed decrease for a crawler with a transverse wave. However, such an effect on the locomotion speed vanishes at the leading order for a crawler with a longitudinal wave. The locomotion velocity without time averaging is on the order of $O(\epsilon^2)$ and $O(\epsilon)$ for the transverse and longitudinal waves, respectively. The time-averaged locomotion velocity, however, becomes on the order of $O(\epsilon^2)$ for both cases.

VI. CONCLUSIONS

In this study, we theoretically analyzed a model crawler on a lubricating viscous fluid with spatial heterogeneity, focusing on multiple timescale mechanics emergent from body-environment coupling. First, we derived a generalized locomotion velocity formula [Eq. (27)] for a lubricating incompressible Newtonian fluid with spatial viscosity variations and then explicitly calculated asymptotic locomotion velocities with small surface deformations for various situations, including a sharp viscosity interface (jump) and linear viscosity gradient, as summarized in Table I. Specifically, we examined a crawler with a self-deformation represented by a traveling wave in both the transverse and longitudinal directions.

In the absence of spatial viscosity variations, the surface deformation with a transverse wave led to a retrograde crawler, moving in a direction opposite to the deformation wave, whereas the longitudinal wave led to a direct crawler whose locomotion velocity had the same direction as the deformation wave. The longitudinal wave can be considered as a contractile wave driven by surface muscular actuation. Therefore, our study implies that the Newtonian fluid alone can account for both types of crawling by altering the surface deformation mode [14]. Indeed, other mechanisms, such as the non-Newtonian properties of fluids [26,27], the elasticity of crawlers themselves [29,31], and control of anchoring phases [13,14], can also contribute to complex modes in the locomotion of biological crawlers. Our study illustrates the general importance of contractile waves in the crawling dynamics.

We then examined the effects of a sharp viscosity jump by calculating time-averaged locomotion velocities in the presence of spatial viscosity variations. For a longitudinal wave, the correction in the locomotion speed from the viscosity jump appears as an oscillation term on the order of $O(A_x) = O(\epsilon)$ in the instantaneous velocity. For a transverse wave, conversely, the correction term is on the order of $O(A_y^2) = O(\epsilon^2)$.

Naive averaging over the phase of oscillation (i.e., ωt and $2\omega t$) in the instantaneous velocity while the current position x_* is fixed often leads to no correction terms from the spatial variation. Hence, to properly accumulate the fast oscillatory effects, we applied multiple timescale analysis to the obtained theoretical expression of the average speed of a crawler in the slow timescale. Remarkably, the resultant asymptotic of the average velocity has a similar form in both cases [Eqs. (68) and (84)], demonstrating that the locomotion speed decreases when the front of the crawler penetrates into the high-viscosity region and when the rear of the crawler exits from the high-viscosity region.

We then analyzed the crawling dynamics with a linear viscosity gradient in space to derive the average locomotion velocity by the multiple timescale analysis, leading to a speed reduction in the transverse wave case. In contrast, the correction term was found to be at the subleading order for the longitudinal wave case, suggesting the great complexity and diversity of the body-environment coupling that depends on the details of the problem settings.

In fact, the medium viscosity can drastically increase with additional solute, and in a laboratory experiment for *Chlamydomonas* viscotaxis, for example, a sharp viscosity interface with viscosity ratio of 60 was realized by a microfluidics device with a 0.75% methylcellusose medium [37].

Even in a higher-viscosity medium, microswimmers such as sperm cells can migrate by modulating their waveform in a solution with 1400 times the viscosity of water [78]. In a biological context, therefore, a viscosity interface may be realized when a crawler moves over a wet substrate with different viscosity from its mucus. The spatial viscosity variations may also be observed when the solute diffuses in the lubricating fluid layer and the linear viscosity variation can also be relevant in biological locomotion. Besides, temperature variations also change the fluid viscosity [72], and the inhomogeneous viscosity profile may also be achieved by controlled heat of the substrate in laboratory experiments. Moreover, our theoretical prediction for the dynamics of crawling locomotion can be potentially testable with robots that mimic gastropod locomotion [15,17,18].

Millimeter-sized nematodes, *Caenorhabditis elegans*, can also migrate through a highly viscous medium, while they exhibit crawling on a gel. Their undulatory waveforms are gradually modulated by the increase of viscosity [79], suggesting adaptation to external mechanical loads in the outer environment [80]. Our results here may offer a methodological basis for understanding this adaptive locomotion in complex environments.

The current crawling model in the lubrication regime is theoretically equivalent to microswimming dynamics in the vicinity of a wall boundary, such as the slithering locomotion of sperm cells [81,82] and gliding motion of bacteria [83,84]. We showed in Sec. III that the leading-order locomotion velocity of the longitudinal wave is the same as that of the Taylor sheet model [73]. Along this line, Du *et al.* [85] addressed the Taylor sheet in viscous two-phase fluids and found a reduction in swimming velocity compared to that in single-phase fluids, although direct comparisons with the current study are not feasible due to the different problem settings. Further studies with various locomotion modes and environment models are warranted for a comprehensive understanding of locomotion with spatial viscosity variation.

More generally, biological locomotion is, in principle, achieved by repeated deformation of a body, and in particular in a dissipation-dominating regime, such as swimming at low Reynolds number and crawling on a thin liquid film, the timescales of shape deformation and progressive movement are well separated due to the inefficiency of locomotion in this regime. Our study highlights the nonlinear, accumulative effects of mechanical coupling between the locomotor and the outer environment with spatial variations. Our methodology based on the multiple timescale analysis will be widely useful for understanding locomotion in complex environments with spatial heterogeneity.

ACKNOWLEDGMENTS

K.I. acknowledges the Japan Society for the Promotion of Science (JSPS) KAKENHI (Grants No. 21H05309 and No. 24K21517) and the Japan Science and Technology Agency (JST) FOREST (Grant No. JPMJFR212N) for funding support.

DATA AVAILABILITY

The data are not publicly available. The data are available from the authors upon reasonable request.

[1] S. Vogel, *Life in Moving Fluids: The Physical Biology of Flow-Revised and Expanded, 2nd ed.* (Princeton University Press, Princeton, 1994).

[2] J. Gray, *Animal Locomotion* (Norton, New York, 1968).

[3] R. M. Alexander and G. Goldspink, *Mechanics and Energetics of Animal Locomotion* (Chapman and Hall, London, 1977).

[4] J. Brackenbury, Fast locomotion in caterpillars, J. Insect Physiol. **45**, 525 (1999).

[5] K. J. Quillin, Kinematic scaling of locomotion by hydrostatic animals: ontogeny of peristaltic crawling by the earthworm *Lumbricus terrestris*, J. Exp. Biol. **202**, 661 (1999).
[6] R. M. Alexander, *Principles of Animal Locomotion* (Princeton University Press, Princeton, 2003).
[7] G. Chapman, Of the movement of worms, J. Exp. Biol. **27**, 29 (1950).
[8] J. B. Keller and M. S. Falkovitz, Crawling of worms, J. Theor. Biol. **104**, 417 (1983).
[9] N. Bolotnik, M. Pivovarov, I. Zeidis, and K. Zimmermann, The undulatory motion of a chain of particles in a resistive medium, Z. Angew. Math. Mech. **91**, 259 (2011).
[10] M. W. Denny and J. M. Gosline, The physical properties of the pedal mucus of the terrestrial slug, *Ariolimax columbianus*, J. Exp. Biol. **88**, 375 (1980).
[11] M. W. Denny, A quantitative model for the adhesive locomotion of the terrestrial slug, *Ariolimax columbianus*, J. Exp. Biol. **91**, 195 (1981).
[12] A. DeSimone, F. Guarnieri, G. Noselli, and A. Tatone, Crawlers in viscous environments: Linear vs nonlinear rheology, Int. J. Non Linear Mech. **56**, 142 (2013).
[13] Y. Tanaka, K. Ito, T. Nakagaki, and R. Kobayashi, Mechanics of peristaltic locomotion and role of anchoring, J. R. Soc. Interface. **9**, 222 (2012).
[14] S. Kuroda, I. Kunita, Y. Tanaka, A. Ishiguro, R. Kobayashi, and T. Nakagaki, Common mechanics of mode switching in locomotion of limbless and legged animals, J. R. Soc. Interface. **11**, 20140205 (2014).
[15] B. Chan, N. J. Balmforth, and A. E. Hosoi, Building a better snail: Lubrication and adhesive locomotion, Phys. Fluids **17**, 113101 (2005).
[16] J. Wilkening and A. E. Hosoi, Shape optimization of a sheet swimming over a thin liquid layer, J. Fluid Mech. **601**, 25 (2008).
[17] B. Chan, S. Ji, C. Koveal, and A. E. Hosoi, Mechanical devices for snail-like locomotion, J. Intell. Mater. Syst. Struct. **18**, 111 (2007).
[18] R. H. Ewoldt, A. E. Hosoi, and G. H. McKinley, Nonlinear viscoelastic biomaterials: meaningful characterization and engineering inspiration, Integr. Comp. Biol. **49**, 40 (2009).
[19] S. L. Miller, The classification, taxonomic distribution, and evolution of locomotor types among prosobranch gastropods, J. Molluscan Stud. **41**, 233 (1974).
[20] J. M. D. Olmsted, Notes on the locomotion of certain Bermudian mollusks, J. Exp. Zool. **24**, 223 (1917).
[21] H. D. Jones and E. R. Trueman, Locomotion of the limpet, *Patella vulgata* L, J. Exp. Biol. **52**, 201 (1970).
[22] J. H. Lai, J. C. del Alamo, J. Rodríguez-Rodríguez, and J. C. Lasheras, The mechanics of the adhesive locomotion of terrestrial gastropods, J. Exp. Biol. **213**, 3920 (2010).
[23] M. Denny, The role of gastropod pedal mucus in locomotion, Nature (London) **285**, 160 (1980).
[24] S. P. Holmes, A. Cherrill, and M. S. Davies, The surface characteristics of pedal mucus: a potential aid to the settlement of marine organisms? J. Mar. Biol. Assoc. UK **82**, 131 (2002).
[25] D. F. Katz, On the propulsion of micro-organisms near solid boundaries, J. Fluid Mech. **64**, 33 (1974).
[26] E. Lauga and A. E. Hosoi, Tuning gastropod locomotion: Modeling the influence of mucus rheology on the cost of crawling, Phys. Fluids **18**, 113102 (2006).
[27] S. S. Pegler and N. J. Balmforth, Locomotion over a viscoplastic film, J. Fluid Mech. **727**, 1 (2013).
[28] M. Argentina, J. Skotheim, and L. Mahadevan, Settling and swimming of flexible fluid-lubricated foils, Phys. Rev. Lett. **99**, 224503 (2007).
[29] N. J. Balmforth, D. Coombs, and S. Pachmann, Microelastohydrodynamics of swimming organisms near solid boundaries in complex fluids, Q. J. Mech. Appl. Math. **63**, 267 (2010).
[30] P. W. Miller and J. Dunkel, Gait-optimized locomotion of wave-driven soft sheets, Soft Matter **16**, 3991 (2020).
[31] M. Iwamoto, D. Ueyama, and R. Kobayashi, The advantage of mucus for adhesive locomotion in gastropods, J. Theor. Biol. **353**, 133 (2014).
[32] S. Lee, J. W. Bush, A. E. Hosoi, and E. Lauga, Crawling beneath the free surface: Water snail locomotion, Phys. Fluids **20**, 082106 (2008).
[33] D. Crowdy, S. Lee, O. Samson, E. Lauga, and A. E. Hosoi, A two-dimensional model of low-Reynolds number swimming beneath a free surface, J. Fluid Mech. **681**, 24 (2011).
[34] S. Joo, S. Jung, S. Lee, R. H. Cowie, and D. Takagi, Freshwater snail feeding: lubrication-based particle collection on the water surface, J. R. Soc. Interface. **17**, 20200139 (2020).

[35] Z. Huang, H. Yang, K. Xu, J. Wu, and J. Zhang, Collecting differently sized particles on water surface by maneuvering pedal waves on the foot of the water snail *Pomacea canaliculata*, Soft Matter **18**, 7850 (2022).

[36] K. M. Wheeler, G. Cárcamo-Oyarce, B. S. Turner, S. Dellos-Nolan, J. Y. Co, S. Lehoux, R. D. Cummings, D. J. Wozniak, and K. Ribbeck, Mucin glycans attenuate the virulence of *Pseudomonas aeruginosa* in infection, Nat. Microbiol. **4**, 2146 (2019).

[37] S. Coppola and V. Kantsler, Green algae scatter off sharp viscosity gradients, Sci. Rep. **11**, 399 (2021).

[38] B. Liebchen, P. Monderkamp, B. ten Hagen, and H. Löwen, *Viscotaxis*: Microswimmer navigation in viscosity gradients, Phys. Rev. Lett. **120**, 208002 (2018).

[39] M. R. Stehnach, N. Waisbord, D. M. Walkama, and J. S. Guasto, Viscophobic turning dictates microalgae transport in viscosity gradients, Nat. Phys. **17**, 926 (2021).

[40] K. Shoele and P. S. Eastham, Effects of nonuniform viscosity on ciliary locomotion, Phys. Rev. Fluids **3**, 043101 (2018).

[41] C. Datt and G. J. Elfring, Active particles in viscosity gradients, Phys. Rev. Lett. **123**, 158006 (2019).

[42] V. A. Shaik and G. J. Elfring, Hydrodynamics of active particles in viscosity gradients, Phys. Rev. Fluids **6**, 103103 (2021).

[43] J. Gong, V. A. Shaik, and G. J. Elfring, Swimming efficiency in viscosity gradients, J. Fluid Mech. **998**, A2 (2024).

[44] T. Kobayashi and R. Yamamoto, Viscotaxis of chiral microswimmer in viscosity gradients, J. Fluid Mech. **1013**, A42 (2025).

[45] P. S. Eastham and K. Shoele, Axisymmetric squirmers in Stokes fluid with nonuniform viscosity, Phys. Rev. Fluids **5**, 063102 (2020).

[46] J. Gong, V. A. Shaik, and G. J. Elfring, Active spheroids in viscosity gradients, J. Fluid Mech. **984**, A26 (2024).

[47] G. I. Taylor, Analysis of the swimming of microscopic organisms, Proc. R. Soc. London A **209**, 447 (1951).

[48] R. Dandekar and A. M. Ardekani, Swimming sheet in a viscosity-stratified fluid, J. Fluid Mech. **895**, R2 (2020).

[49] C. Kamal and E. Lauga, Resistive-force theory of slender bodies in viscosity gradients, J. Fluid Mech. **963**, A24 (2023).

[50] C. E. López and E. Lauga, Rate invariance and scallop theorem in viscosity gradients, Phys. Rev. Fluids **8**, 063301 (2023).

[51] Z. Liu, Y. Chao, Z. Zheng, and L. Zhu, Spontaneous oscillation of an active filament under viscosity gradients, Soft Matter **20**, 3845 (2024).

[52] S. Anand, J. Elgeti, and G. Gompper, Viscotaxis of beating flagella, Soft Matter **21**, 3228 (2025).

[53] J. Gonzalez-Gutierrez, S. Osorio-Ramirez, F. J. Solorio-Ordaz, and R. Zenit, Dynamics of a helical swimmer crossing an interface between two immiscible fluids, Phys. Rev. Fluids **4**, 083102 (2019).

[54] C. Esparza López, J. Gonzalez-Gutierrez, F. Solorio-Ordaz, E. Lauga, and R. Zenit, Dynamics of a helical swimmer crossing viscosity gradients, Phys. Rev. Fluids **6**, 083102 (2021).

[55] C. Feng, J. J. Molina, M. S. Turner, and R. Yamamoto, Dynamics of microswimmers near a liquid–liquid interface with viscosity difference, Phys. Fluids **35**, 051903 (2023).

[56] J. Gong, V. A. Shaik, and G. J. Elfring, Active particles crossing sharp viscosity gradients, Sci. Rep. **13**, 596 (2023).

[57] K. Ishimoto, H. Gadêlha, E. A. Gaffney, D. J. Smith, and J. Kirkman-Brown, Coarse-graining the fluid flow around a human sperm, Phys. Rev. Lett. **118**, 124501 (2017).

[58] J. S. Guasto, K. A. Johnson, and J. P. Gollub, Oscillatory flows induced by microorganisms swimming in two dimensions, Phys. Rev. Lett. **105**, 168102 (2010).

[59] B. M. Friedrich and F. Jülicher, Chemotaxis of sperm cells, Proc. Natl. Acad. Sci. USA **104**, 13256 (2007).

[60] K. Shiba, S. A. Baba, T. Inoue, and M. Yoshida, Ca^{2+} bursts occur around a local minimal concentration of attractant and trigger sperm chemotactic response, Proc. Natl. Acad. Sci. USA **105**, 19312 (2008).

[61] K. Drescher, R. E. Goldstein, and I. Tuval, Fidelity of adaptive phototaxis, Proc. Natl. Acad. Sci. USA **107**, 11171 (2010).

[62] H. de Maleprade, F. Moisy, T. Ishikawa, and R. E. Goldstein, Motility and phototaxis of *Gonium*, the simplest differentiated colonial alga, Phys. Rev. E **101**, 022416 (2020).
[63] B. J. Walker, K. Ishimoto, E. A. Gaffney, C. Moreau, and M. P. Dalwadi, Effects of rapid yawing on simple swimmer models and planar Jeffery's orbits, Phys. Rev. Fluids **7**, 023101 (2022).
[64] E. A. Gaffney, M. P. Dalwadi, C. Moreau, K. Ishimoto, and B. J. Walker, Canonical orbits for rapidly deforming planar microswimmers in shear flow, Phys. Rev. Fluids **7**, L022101 (2022).
[65] M. P. Dalwadi, C. Moreau, E. A. Gaffney, K. Ishimoto, and B. J. Walker, Generalised Jeffery's equations for rapidly spinning particles. Part 1. Spheroids, J. Fluid Mech. **979**, A1 (2024).
[66] M. P. Dalwadi, C. Moreau, E. A. Gaffney, B. J. Walker, and K. Ishimoto, Generalised Jeffery's equations for rapidly spinning particles. Part 2. Helicoidal objects with chirality, J. Fluid Mech. **979**, A2 (2024).
[67] B. J. Walker, K. Ishimoto, C. Moreau, E. A. Gaffney, and M. P. Dalwadi, Emergent rheotaxis of shape-changing swimmers in Poiseuille flow, J. Fluid Mech. **944**, R2 (2022).
[68] B. J. Walker, K. Ishimoto, and E. A. Gaffney, Systematic parameterizations of minimal models of microswimming, Phys. Rev. Fluids **8**, 034102 (2023).
[69] O. Reynolds, IV. On the theory of lubrication and its application to Mr. Beauchamp Tower's experiments, including an experimental determination of the viscosity of olive oil, Philos. Trans. R. Soc. **177**, 157 (1886).
[70] A. Cameron, *Principles of Lubrication* (Longman Publishing Group, London, 1986).
[71] L. G. Leal, *Advanced Transport Phenomena: Fluid Mechanics and Convective Transport Processes* (Cambridge University Press, Cambridge, 2007), Vol. 7.
[72] N. Oppenheimer, S. Navardi, and H. A. Stone, Motion of a hot particle in viscous fluids, Phys. Rev. Fluids **1**, 014001 (2016).
[73] J. R. Blake, Infinite models for ciliary propulsion, J. Fluid Mech. **49**, 209 (1971).
[74] A. DeSimone and A. Tatone, Crawling motility through the analysis of model locomotors: Two case studies, Eur. Phys. J. E **35**, 85 (2012).
[75] H. W. Lissmann, The mechanism of locomotion in gastropod molluscs: I. Kinematics, J. Exp. Biol. **21**, 58 (1945).
[76] H. W. Lissmann, The mechanism of locomotion in gastropod molluscs: II. Kinetics, J. Exp. Biol. **22**, 37 (1945).
[77] J. R. Vélez-Cordero and E. Lauga, Waving transport and propulsion in a generalized Newtonian fluid, J. Non-Newtonian Fluid Mech. **199**, 37 (2013).
[78] D. J. Smith, E. A. Gaffney, H. Gadêlha, N. Kapur, and J. C. Kirkman-Brown, Bend propagation in the flagella of migrating human sperm, and its modulation by viscosity, Cell Motil. Cytoskeleton **66**, 220 (2009).
[79] C. Fang-Yen, M. Wyart, J. Xie, R. Kawai, T. Kodger, S. Chen, Q. Wen, and A. D. T. Samuel, Biomechanical analysis of gait adaptation in the nematode *Caenorhabditis elegans*, Proc. Natl. Acad. Sci. USA **107**, 20323 (2010).
[80] K. Ishimoto, C. Moreau, and J. Herault, Robust undulatory locomotion through neuromechanical adjustments in a dissipative medium, J. R. Soc. Interface. **22**, 20240688 (2025).
[81] R. Nosrati, A. Driouchi, C. M. Yip, and D. Sinton, Two-dimensional slither swimming of sperm within a micrometre of a surface, Nat. Commun. **6**, 8703 (2015).
[82] S. Unnikrishnan, R. L. Scott, E. Ogundele, M. A. Azad, K. Ishimoto, S. S. Suarez, and C. K. Tung, Hybrid motility mechanism of sperm at viscoelastic fluid-solid interface, Sci. Rep. **14**, 21841 (2024).
[83] R. W. O'Brien, The gliding motion of a bacterium: *Flexibacter* strain *BH*3, ANZIAM J. **23**, 2 (1981).
[84] A. M. Siddiqui, R. P. Burchard, and W. H. Schwarz, An undulating surface model for the motility of bacteria gliding on a layer of non-Newtonian slime, Int. J. Non Linear Mech. **36**, 743 (2001).
[85] J. Du, J. P. Keener, R. D. Guy, and A. L. Fogelson, Low-Reynolds-number swimming in viscous two-phase fluids, Phys. Rev. E **85**, 036304 (2012).